공학석사학위논문

MPL 물성특성 변화에 따른 고분자 전해질 연료전지 성능개선에 관한 연구

Experimental Study on the Effects of MPL Material Properties in PEM Fuel Cell

2018 년 8 월

서울대학교 대학원

기계항공공학부

송 병 근

Acknowledgement

First and foremost, I would like to express my respect and appreciation to my advisor, Professor Kyoungdoug Min. During the journey of my graduate course, my knowledge and personality have grown with the help of his invaluable teachings and advice. He provided the inspirations of this study, and his guidance and encouragement were the power to overcome numerous difficulties during the research. Without his guidance, this accomplishment would not have been possible. I extend my appreciation to Seoul National University and the committee members, Professor Min Su Kim and Seung Hwan Ko. Thank you for your advices and comments on my thesis topic. You truly enriched and completed this work.

I would like to express my appreciation to the fuel cell stack project members, Dr. Hwanyoung Oh, Yoo-il Lee, Keven Lee, and Jaehyun Choi for your invaluable assistances, intriguing discussions and delightful memories. You provided endless inspirations and knowledge into my research topic.

Also to all of the laboratory members, I learnt from each one of you. Insuk Ko, Youngbok Lee, Seunghyup Shin, Woojae Kim, and Junghyun Kim, I learnt from your great personality. I also learnt from Yongjoo Lee, Dr. Seokwon Cho, and Sanghyun Chu from your hard works, Jongwon Chung, and Sunyoung Moon, from your great diligence, Hyunjung Oh, Hyungjin Shin, JiHwan Park, Sejin Song, Sukwon Shin, and Jaehyun Choi, from your great aptitude to learn. Seung-il Lee, Taewoo Nam and Chiheon Song from your smartness. And of course, Cheonghwan Kim, from your amazing dancing skills.

Also, my gratitude goes to the StarCraft colleagues, Dr. Gyujin Kim, Sanghyun Chu, and Taewoo Nam. Although you still haven't reached the right amount of workmanship to stimulate my tension, it was always a great way to recharge myself to continue on my graduate course.

It was an honor and a pleasure to have opportunity to be able to work with JNTG. I'd like to thank Dr. EunSook Lee, Dr. Jy-Young Jyoung for material support and valuable comments. This work would not have been completed from their enthusiastic passion and knowledge on this field.

Lastly, I'd like to present the deepest respect and gratitude to my parents. You have given up and missed so many good things to take care of us and to support my education. Your dedication will always be remembered. Thank you.

Abstract

Experimental Study on the Effects of MPL Material Properties in PEM Fuel Cell

ByungGun Song
Department of Mechanical and Aerospace Engineering
The Graduate School
Seoul National University

A sluggish oxygen reduction at the cathode side of a Polymer electrolyte membrane fuel cell (PEMFC) has a critical effect on its performance. Amelioration of the oxygen reduction can be achieved by improving the oxygen transportation, so the oxygen concentration at the catalyst layer remains equally distributed. Better oxygen transportation can be achieved by improving the mechanical properties of micro porous layer (MPL). In this study, the effects on a fuel cell performance of the MPL samples of various material properties are experimentally compared and optimized; Oxygen transport resistance and water management capability were analyzed by polarization curve, Electrochemical Impedance Spectroscopy (EIS) model and by measuring the limiting current density.

This study focused on the performance amelioration of PEMFC by varying the material property of MPL which is one of the key components. Purpose of the research is also to prove the causes of effects of such performance enhancements academically and the point of improvement is expected in 3 aspects.

(1) Improved oxygen transportation in cathode side

(2) Enhanced water removal through MPL

(3) Improvement of electrical conductivity as an electrode

With the technological backgrounds of enhanced PEMFC performance, water removal capability carries a vital role in its performance. Thus, the design parameters of MPL and experimental conditions are focused on humidified and betterment of water removal condition. It is proven through previous research that characteristic of MPL plays dominant role on PEMFC capillary action and oxygen transportation. Therefore, this study utilized three types of carbon powder to manufacture MPL slurries of various material properties.

First, pore size graded MPL slurries are manufactured with two different carbon powers (A6, A3) of different particle sizes. Polarization curve response demonstrated an enhanced concentration voltage loss region with larger pore size diameter. Oxygen transport resistance is calculated through measuring the limiting current density response to find causes of such improvement. Under the specific experimental condition, it is proven that oxygen transportation is not affected by different pore size diameter of MPL. In fact, increment of pore size diameter lowers the capillary pressure to ease out the water discharge through GDL.

With A6 type carbon powder which depicted an improved performance in high-humidified conditions, carbon type C content of superior electrical conductivity was gradually added. EIS analysis confirms the gradual decrement of ohmic resistance along that of C type content. However, C type, instead of being highly conductive, had surface area of 10 times higher than that of A6. It was shown that initiation of the concentration loss being advanced in both I-V response and EIS

analysis in concentration voltage loss. With such response, addition of carbon type C was utilized to adjust a power density enhancement regarding such trade-off relations.

Material characteristics are quantitatively analyzed through Ex-situ experiments such as Scanning electron microscope (SEM) material analysis, mercury intrusion porosimetry and measurement of contact angle between water droplet and MPL surface. Among experimental samples, carbon compound of A6 with 3 wt. % of C type content demonstrated the best performance among experimental samples, and the power density was improved by factor of 1.16 compared to the commercial sample.

This study quantitatively analyzes the development of the performance change of various MPL material properties based on academic theories. Causes of effects are revealed through results of EIS analysis, limiting current density response and regarding scientific theories. Such results are expected to contribute further research and development of MPL and compatible components of PEMFC.

Keywords: Micro Porous Layer (MPL), PEMFC water management, Electrochemical Impedance Spectroscopy (EIS), Limiting Current Density (LCD), Oxygen transport resistance.

Student Number: 2016-23285

Contents

List of Tables

List of Figures

Nomenclature

A_i	active area [m^2]
ASR	area specific resistance [$\Omega\ m^2$]
C_i	molar concentration [mol m^{-3}]
d_p	pore size diameter [nm]
D_i	diffusion coefficient [m^2s^{-1}]
D_{ij}	binary gas phase diffusion coefficient [m^2s^{-1}]
E_0	thermodynamically predicted fuel cell voltage output [V]
F	Faraday's constant [96,485 C mol^{-1}]
j	current density [A m^{-2}]
K_{knud}	Knudsen number [-]
M_i	molar mass [g mol^{-1}]
n_i	number of molecules per unit volume [m^{-3}]
N_i	molar flux rate per unit area [mol $m^{-2}s^{-1}$]
P_{sat}	saturated water vapor pressure [kPa]
P	Pressure [kPa]
r_h	relative humidity [-]
r_i	molecular collision diameter
R	gas constant [8.134 J mol^{-1} K^{-1}]
R_i	resistance [V A^{-1}] / oxygen transport resistance [s m^{-1}]
$\hat{s}$	Entropy [kJ mol^{-1}]
t	time [s]
T	temperature [K]
v_i	diffusion volume [-]
w	characteristic frequency [Hz]
x	mole fraction [-]
Z	impedance [$\Omega\ cm^2$]

Greek Letters

α	charge transfer coefficient [-]
η_i	overvoltage [V]
θ	contact angle [degrees]
γ	specific heat ratio [-]
ρ	gas density [kg m^{-3}]
τ	tortuosity [-]
λ	water content in membrane [-]
σ	surface tension [Nm^{-1}]

Subscripts/Superscripts

ct	charge transfer
PEM	polymer electrolyte membrane
ion	ionomer
Knud	Knudsen diffusion
lim	value at limiting current density
f	faradaic
MD	molecular diffusion
ORR	oxygen reduction reaction
HOR	hydrogen oxidation reaction
Pt	platinum
max	maximum

Chapter 1. Introduction

1.1 Backgrounds and Motivations

1.1.1 Technological background of PEMFC

After years of world wise interest and efforts, PEMFC is at the commercialization stage now with the achievement of enormous performance incensement [1-4]. Consequently, successful launchings of Honda Clarity (2008), Toyota Mirai (2014), and Hyundai Nexo (2018) are coming along. There have been significant milestones that enhanced fuel cell performance in a decade period. Of which, a perennial issue of oxygen dispersion and water retention at cathode channel has been enhanced by applying the 3-D mesh type flow channel [4]. By utilizing a new channel shown in figure 1.1, generated water dragged up to the channel is quickly removed through the 3D mesh flow field. Electrolyte-Membrane-Assembly also solved its weakness of platinum particles not being fully utilized by replacing hollow carbon support to the solid core type. MEA now has increased the oxygen reduction rate by factor of 1.8 [3].

With such accomplishments, PEM fuel cells are now capable of producing more current per unit area compared to that of a decade ago. Improved current densities at operating voltage stands as more water generation as by-product. Thus, a modern design index for the fuel cell components is required. Of which, gas diffusion layer (GDL) is one of the key component of fuel cell that majorly affects the fuel cell performance. GDL is composed of two layers; it is composed of gas diffusion backing layer (GDBL) and micro porous layer (MPL). In previous research, it is known that MPL plays critical role when it comes to water management and oxygen transportation [5].

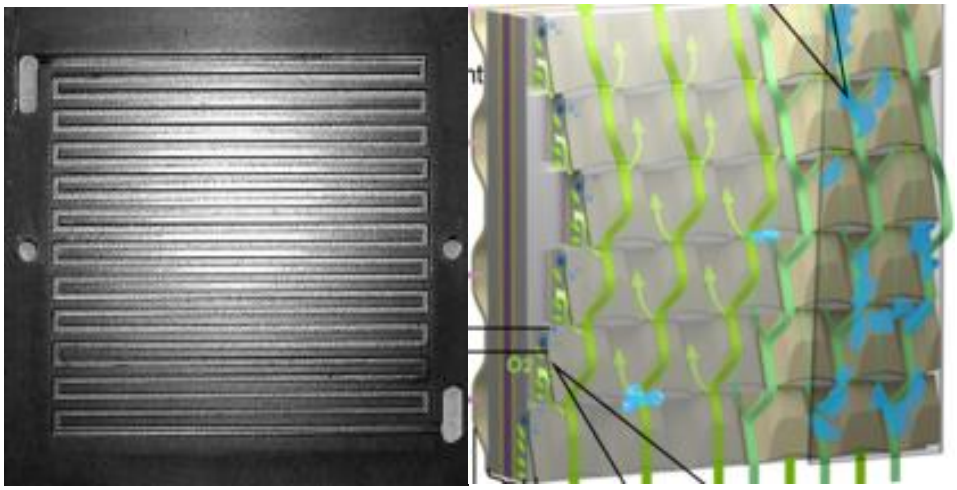

Figure 1.1 Serpentine and 3D-fine mesh applied in Toyota *Mirai* [4]

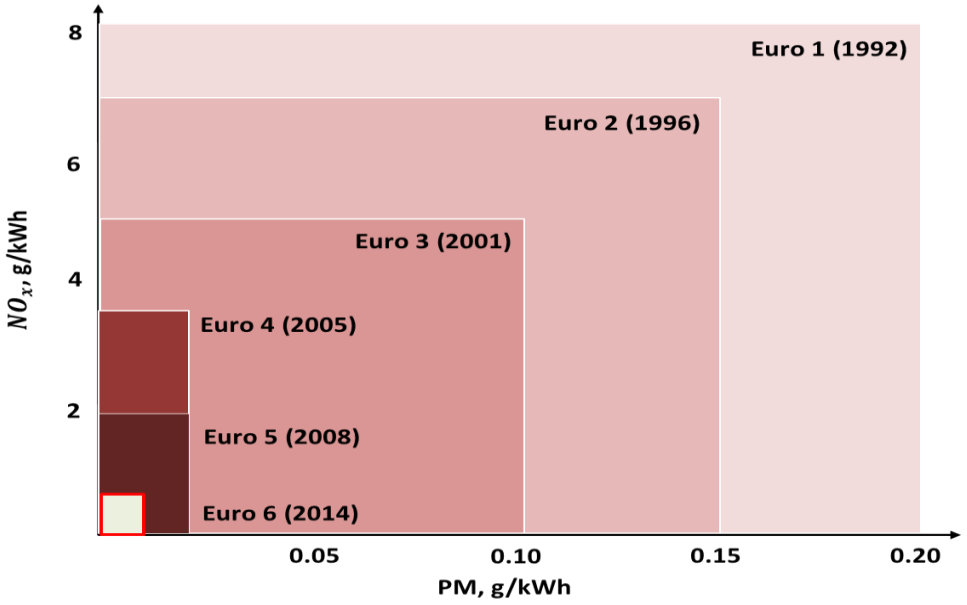

Figure 1.2 European Regulation Standards on the Diesel Vehicle emissions [6]

Chan proposed three possible power sources for the future motor market [1]. They are hybrid, electric and fuel cell vehicle. Fuel cell vehicle market is growing steeply over years and soon will take a certain portion in total vehicle market. Several reasons verify the background of upcoming prominent technology.

First, government regulations of vehicle emissions and mileage have been reinforced over decades. Especially in 2017, application of Euro 6c regulation is requiring a real driving emissions test [6] for a vehicle to be on market. Figure 1.2 demonstrates how dramatically governments sets the requirements regarding emissions for a vehicle to be released. To satisfy the regulation, the price of internal combustion engine-based vehicles will dramatically increase.

Not only the emissions regulation but also CO_2 regulation is a problem that motor companies must face because of CO_2 and emissions trade-off relation. Inevitably internal combustion-based vehicles will have to raise the price with the pricy attachments. As an alternative, eco-friendly vehicles are getting attention world wise. For several years, electrical motor sale increased steeply. However, researchers suggest that electrical vehicle is not a solution as the replacement for fossil fuel [1]. Including the well-to-wheel efficiency issue, electric vehicles are still facing serious problems with especially batteries. Lithium ion battery, which is a major power source for the electrical vehicle, has a limited life span with its dissipation rate and demerits of its charging time.

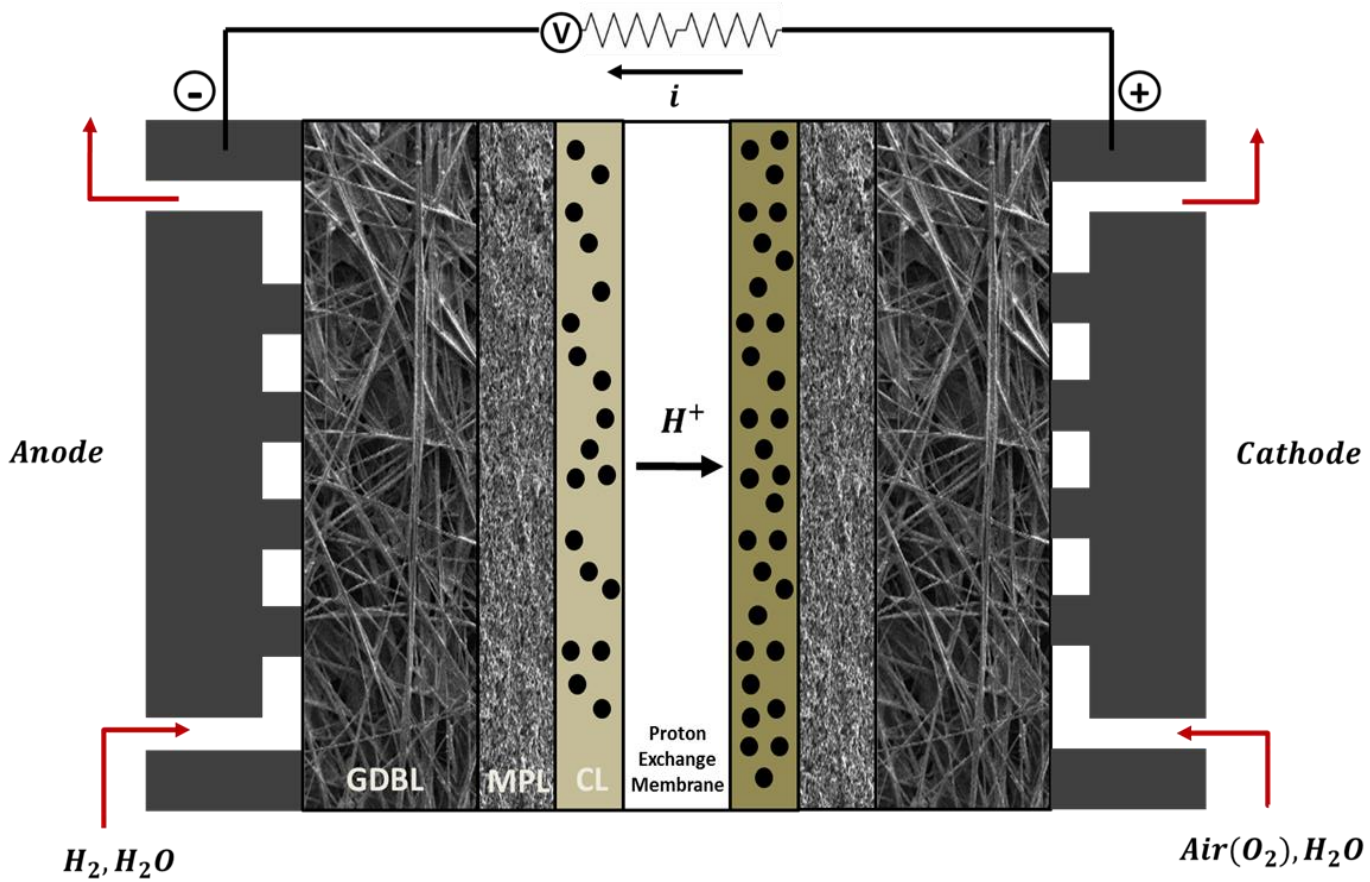

Figure 1.3 Schematic of PEMFC operation

1.1.2 PEMFC operation

Among various types of fuel cells, PEMFC is the most suitable for automobiles due to its characteristics of high energy efficiency, zero-emission[7, 8] and for its comparatively low operating temperature below 100℃. PEM fuel cell is an energy generating device which consumes hydrogen and oxygen to generate electricity.

As demonstrated in figure 1.4, PEMFC is composed of numerous components. Each component has to carry out its role in order to have a fuel cell to operate successfully. Also every fuel cell component is related to the voltage loss source due to its electrochemical characteristics. In this chapter, the major voltage losses in fuel cells and how they are related to each component are reviewed. Lastly, more details on gas diffusion layers are considered such as how to ameliorate gas diffusion layers to enhance the fuel cell performance.

1.1.3 Sources of voltage loss in PEMFC

Due to its electrochemical characteristics, fuel cell undergoes three types of voltage losses. Because of non linear I-V response, it is important issue for researcheres in which operating condition should a fuel cell be operated. Before reviewing the voltage loss sources, we must be acknowledged about the potential voltage that a cell obtains due to potential energy of chemicals. Open circuit voltage (OCV) can be described with Nernst equation regarding varying temperature, pressure, and activity.

$$\mathrm{E} = \mathrm{E}^0 + \frac{\Delta \hat{s}}{nF}(\mathrm{T} - \mathrm{T}_0) - \frac{RT}{nF} ln \frac{\prod a_{products}^{v_i}}{\prod a_{reactants}^{v_i}} \qquad (1.1)$$

(1) Activation Voltage Loss

Opencircuit voltage reveals when there is no electricity generation. It only appears due to the chemical potential of hydrogen oxidation and oxygen reduction process. In order to produce electricity out of the system, Activation loss must be proceeded. Modified Butler-Volmer equation describes the activation voltage loss of extremely low current density. Activation loss is predominant in a low current density region.

$$\eta_{\text{act}} = -\frac{RT}{\alpha nF} lnj_0 + \frac{RT}{\alpha nF} lnj \tag{1.2}$$

(2) Ohmic Voltage Loss

Ohmic loss is composed of ionic conductivity and electrical resistance. Ionic conductivity is a resistance of membrane to transport proton generated from anode to the cathode side. Ohmic loss is linearly proportional to the current density of a cell.

$$V_{\text{ohm}} = j \times (ASR_m + R_{elec}) \tag{1.3}$$

(3) Concentration Voltage Loss

Concentration volatge loss is highly related to the flooding and dissipation of the reactant concentration at the catalyst layer. A sudden voltage drop is present for fuel cell performance, and it is considered the most important issue to be ameliorated. Concentration loss is demonstrated in mass transportation loss term.

$$\eta_{\text{conc}} = c \cdot \ln \frac{j_l}{j_L - j} \tag{1.4}$$

Each voltage losses affect in every current density region. However, predominance of them are in different region of the polarization curve. Equation 1.5 shows the simplified voltage loss equation. Each voltage losses are highly related to each other, so it is hard to define a specific component is only related to which over voltage source. However, voltage loss can be simplified and written in terms by its predominance at certain region. As appears in equation 1.5, activation loss is predominant in low current region, and concentration loss is dominant in high current density region.

$$\mathrm{V(I)} = E_{thermo} - aln(I) - R_{ohmic} \cdot \mathrm{I} - \mathrm{ce}^{d \cdot I} \qquad (1.5)$$

1.1.4 Three major roles of Gas Diffusion Layer (GDL)

Although GDL plays numerous roles for fuel cells such as compressing media and aid for membrane humidity, we focused on three critical roles of GDL into the research topic.

(1) Gas transporting media

Diffusion must take over to have gas to reach to the catalyst layer. Thus, GDL porosity is designed to have larger than 70% porosity [9]. By applying gas diffusion layer, we expect the reactants gas to equally distributed to the surface with faster diffusion flux rate [5].

(2) Water exiting media

Not only GDL transports reactants to the catalyst layer but also removes excessive water generates from the catalyst layer backward. Flooding is one of the critical issue that initiates concentration over voltage.

(3) Electrode

GDL is on the way where generated current travels to the current collector. Therefore, despite of being a porous media, it has to still conduct electricity. Increasing the contact area can easily enhance the conductivity of GDL, but such enhancement can bring trade-off for other criteria such as oxygen transportation.

In this paper, correlation of micro porous layer material property and performance of these three roles of GDL are focused into these designing parameters.

1.2 Literature Review

1.2.1 Carbon Material Properties

There have been numbers of efforts to improve fuel cell performance by changing the carbon powder properties. First, there have been studies to control PTFE content and MPL thickness to optimize the cell performance. Researchers including Park and Tseng [10-12] suggested a limitation of PTFE content that increment of PTFE content will induce a severe performance loss. Also, there are numbers of research regarding optimization by controlling carbon blacks. Wang et al. [13] compared two types of carbon powders with opposite characteristics. They compared the characteristics of carbon blacks and measured impedance response of varied composites. Tang and [14] and his co-researchers controlled NH4Cl pore-former to form a porosity-graded MPL while pore diameter remains constant. Chun et al. [15] manufactured pore-graded MPL by mixing thermal expandable graphite (TEG) as additive. Tanuma et al. varied MPL pore size diameter while that of GDBL is constant [16] They introduced the method of varying MPL pore size diameter by utilizing different carbon blacks and suggested larger pore size diameter being able to remove excessive water successfully. Simon et al. found out the pore properties on liquid water transport by measuring the limiting current density [17] However, the result suggested only the possibility of ameliorated concentration voltage loss with the polarization curve, yet there was deficiency of specific analysis of causes of effect at various operating conditions.

1.2.2 Oxygen transportation in PEMFC

One way to analyze the performance of the cell of various MPL properties is analyzing the oxygen transport mechanism in PEMFC. There are numerous previous studies analyzing oxygen transport mechanism by measuring limiting current density [5, 17-19].

Additionally, previous research on investigating oxygen transportation categorized the transportation phenomenon into diffusion mechanisms and ionomer permeation. In this study, analysis on oxygen transportation mechanism focused on molecular diffusion, Knudsen diffusion and transportation through MEA including the ionomer permeations.

Separation of the diffusion component has been studied by numerous researchers. Categorization of the diffusion mechanism has been conducted by changing inert gases and by varying pressure [18, 20-23]. Especially, Beuscher et al. isolated the portion of the molecular diffusion from the total oxygen transport resistance by utilizing air and heliox. By utilizing two different inert gases, they were able to vary the molar mass of the gas injection. This resulted in different limiting current densities which stands for difference of resistance caused by molecular diffusion. Utilization of the air and heliox in cathode side did successfully isolate the molecular diffusion portion, however did not consider the water condensation through the chemical reaction.

Caulk et al [21]. suggested the idea of separating under-saturated region, so oxygen transportation can be experimentally measured without considering the water blockage through the system. He and his co-researchers limited the oxygen concentration to the cathode and figured out that limiting current density can be extracted before the condensation of water. Transport mechanism, then often categorized into Knudsen diffusion and ionomer permeations.

Pt/C agglomeration is surrounded by ionomer film, and the permeability of the ionomer film is stimulated by the relative humidity. Oh et al. figured out that portion of transport resistance that ionomer film takes is over 40% when relative humidity is 30% and exponentially decreases as humidity increment. However, the portion still stands as 18% of the total oxygen transport resistance, and it cannot be ignored. To be able to separate the portion of ionomer resistance, Nonoyama et al. [19] varied relative humidity when measuring the limiting current density. Their findings emphasized the fact that ionomer resistance is a critical source of transporting barrier.

Not only ionomer permeation is the major source that affects limiting current density so is the membrane ionic conductivity. Liu and following referees measured the oxygen transport resistance when the membrane thickness is varied. Membrane thickness is a major source that decides the ionic conductivity, but their findings also suggested that membrane humidity is capable of exponentially increase the conductivity. This study focused on the fact that the water content in membrane is affected by the relative humidity of the inlet gas and will be influential to the limiting current density response. Further membrane characteristics will be discussed in chapter 3 with theories organized by O'hayre et al [24].

1.2.3 Electrochemical Impedance Spectroscopy

PEMFC operation is often under high current density and humidified condition where water condensation takes a critical role in the performance response. Generated water can block the reactant transporting path in various components. Springer et al [25]. measured the AC impedance in dry and humidified condition to investigate the oxygen transporting characteristics.

Analysis on AC impedance was studied by decades. It is normalized that impedance response can be schematically drawn as equivalent circuit model in figure 1-5 [25-28]. EIS technique is utilized to quantitatively analyze the voltage loss at the

specific operating conditions. To specify the voltage loss region, impedance model of Kim et al. [29] was applied. In result, Voltage loss is specified into kinetic, ohmic, and concentration loss.

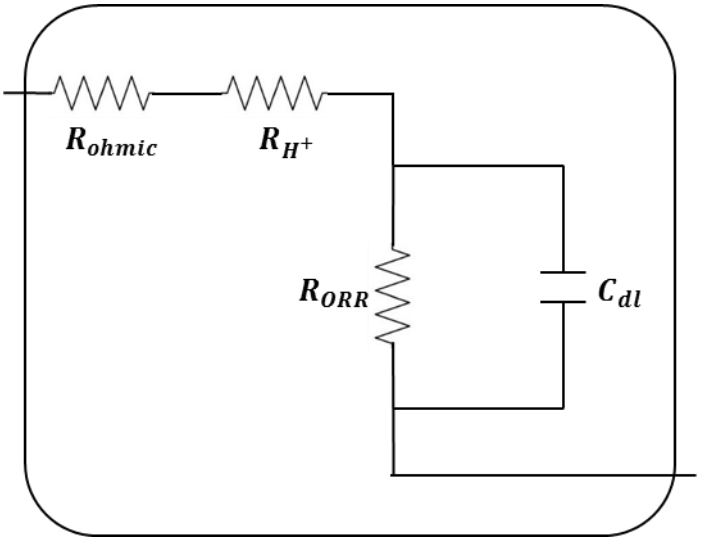

Figure 1.4 Electrochemical circuit model

Impedance model categorizes the experimental response into concentration, ohmic and activation loss region by the response characteristics. Further analysis on the response will be conducted in chapter 2 with the experimental results.

1.3 Research Objectives

Research objectives of the study is to investigate the characteristics of MPL material properties by three in-situ experiments and to analyze the causes of fuel cell responses at various operating conditions. First, MPL samples of various material characteristics are manufactured; pore size diameter is controlled from 50 to 100 nm. Also, conductive carbon content is added from 0 to 10 weight percent with optimized size of base carbon. Manufactured MPL samples are sent to various material analysis institution. SEM material analysis, mercury intrusion porosimetry and measurement of the contact angle are performed to gasp the characteristics. Through the material analysis, MPL hydrophobic property, PTFE characteristics, and their pore size diameters are measured quantitatively. Three different experiments are utilized for comparison among samples. Lastly, experimental results are investigated upon scientific background.

Chapter 2. Methodologies

2.1 Manufactured MPL properties.

2.1.1 Characteristics of utilized carbon blacks

Three types of carbon powders are utilized to manufacture MPL samples on an identical GDBL (JNT30). Two major carbon powder properties are taken account when manufacturing the MPL samples. First, two different carbon blacks of different particle sizes are utilized to result in different pore size diameter. A6 carried twice as bigger particle size as A3 carbon powder. Carbon type C was chosen for the additive to A6 powder for the better electrical conductivity. Carbon C had a characteristic that surface area was 50 times bigger than that of other materials. Chen et al. had utilized the carbon powder, *pearl 2000* to membrane back bone structure, and it had a similar characteristic of huge surface area [30]. Chen concluded increment of the hydrophilic property of the material due to the increasing surface area, so small amount of poor water management was expected, but major concern was to see if increasing electrical conductivity will be the dominant performance increasing factor.

After all, five experimental MPL samples are manufactured on an identical GDBL. Pore size diameter resulted in 50nm and 100nm when A3 and A6 carbon powders are utilized. The schematic of the A3 and A6 MPL are shown in figure 2.1 Also, a carbon powder C with superior conductivity resulted in 100nm pore size diameter.

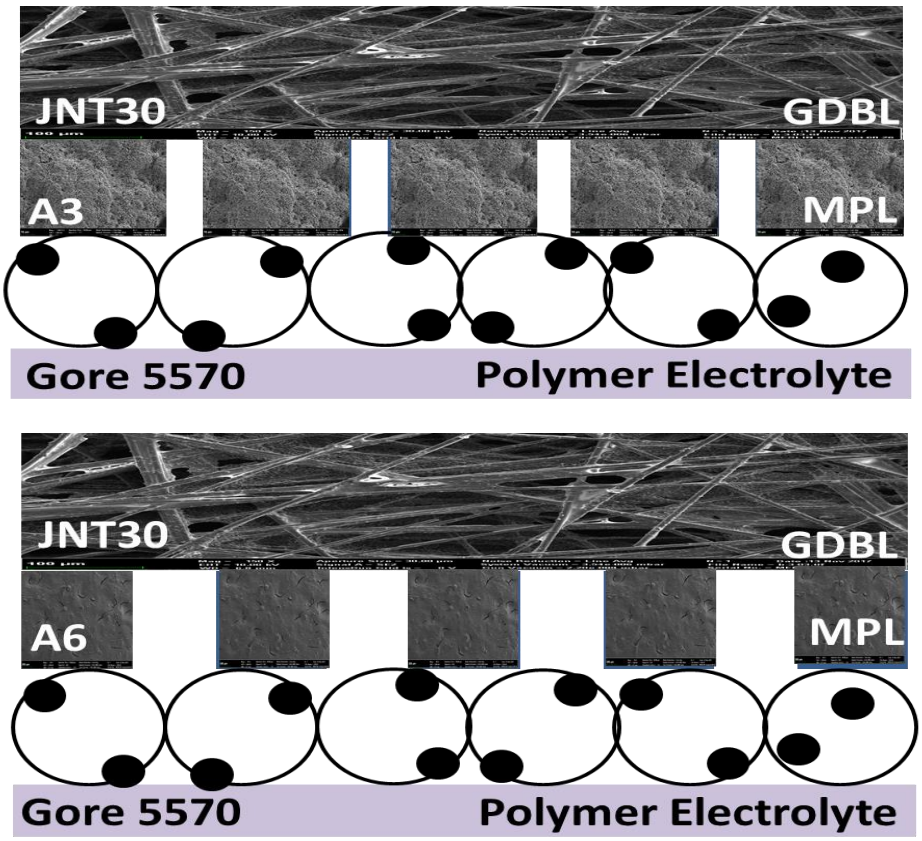

Figure 2.1 Schematic of pore size graded MPL slurries

Table 2.1 Characteristics of utilized carbon powders

Ranking among 3 carbon types	
Particle Size Rank	A6 > A3 ≈ C
Electrical Conductivity Rank	C > A3 ≈ A6
Carbon Surface Area Rank	C >> A3 ≈ A6

Table 2.2 List of experimental GDL samples

Nom	GDBL	Thickness (um)	Pore size (nm)	Porosity (%)	Carbon C (%)
A3	JNT30	308±5	52.3	79.69	0
A6	JNT30	310±5	103.14	82.42	0
A6H	JNT30	309±5	103.12	80.50	3
A6M	JNT30	307±5	103.15	81.77	5
A6L	JNT30	311±5	103.14	79.44	10

2.1.2 Background Theory

MPL material properties are varied into pore size diameter and electrical conductivity by utilizing various type of carbon powders. There is background theory behind the design parameters.

When gas flows through the flow channel, diffusion process takes over at GDL and carries it to the catalyst layer. Diffusion mechanism is often described as Fick's law of diffusion equation 2.1 [31]. Where D stands for the effective diffusion coefficient.

$$J = -D\frac{\partial C}{\partial x} \tag{2.1}$$

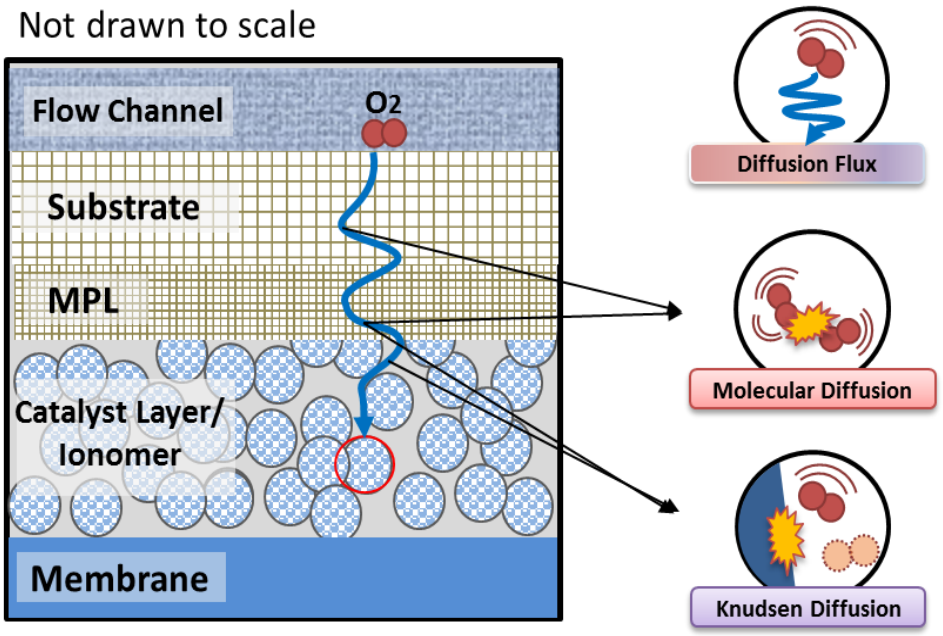

Figure 2.2 Schematic of diffusion mechanism

2.1.2.1 Diffusion Process

Diffusion process can be described into molecular and Knudsen diffusion [19]. Molecular diffusion is diffusion caused by collision among molecules. Table2.7 describes the diffusion coefficient of the molecular diffusion. Its process dominantly occurs in comparatively large pore size [19]. Knudsen diffusion, on the other hand, dominantly exists in small pore size. The work of Nonoyama proves that both Knudsen and molecular diffusion takes place in MPL. Diffusion coefficient is described in Equation in table 2.7. Pore size diameter control in diffusion point of view is targeted that in larger pore diameter will accelerate diffusion process in Knudsen diffusion region.

2.1.2.2 Water removal Capability

Initiation of successful capillary action is a key to improve water removal capability of GDL. Washburn equation defines the Capillary pressure of the hydrophobic media [32]. Work of Simon [17], proves that saturated water in liquid state proceeds predominantly through larger pores of the MPL if the water contact area of media is over 90 degrees. Successful water removal directs that liquid water has to overcome capillary pressure in order to get filled in pores.

$$P_c = P_L - P_v = \frac{4 \cdot \gamma_{H_2O} \cdot \cos\theta}{d_{pore}} \qquad (2.2)$$

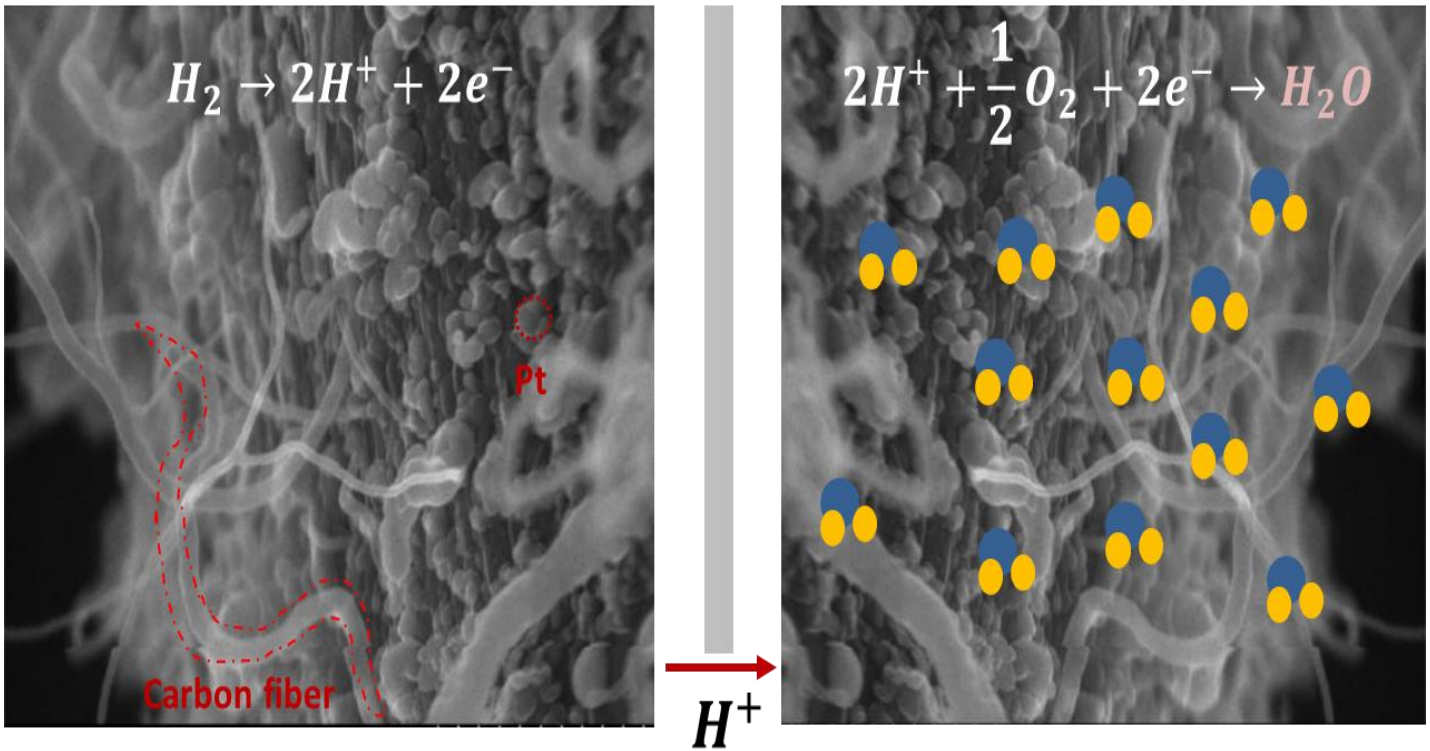

Figure 2.3 Schematic of capillary action in the catalyst layer

2.2 Experimental Methodologies

Experiments are carried out to analyze the performance of varied MPL properties in various aspects. Three different experiments are conducted to compare cell response generally and quantitatively.

First, current-voltage response is measured to grasp overall cell performance. Impedance response is measured and analyzed through EIS technique to analyze the voltage losses in various operating condition. Lastly, limiting current density is measured under condition of no water condensation to explicitly measure oxygen transportation response.

Serpentine channel was utilized on both cathode and anode side. The most typical type of channel is used for two purposes. First, advection through GDBL should be neglected to analyze the water removal capability or the oxygen transportation only. Secondly, water condensation in the channel should be minimized. Cell temperature is maintained to be 65 degrees Celsius, and no additional pressure was applied to the cell beside the compression torque. We utilized non-wetting material gasket to control GDL compression ratio. Identical GDL compression torque and ratios are applied to each sample.

Table 2.3 Common experimental conditions of in-situ experiments

Fixed Parameter	Condition
Channel(Anode/Cathode)	Serpentine/Serpentine
MEA	Gore M5730
Cell Temperature (℃)	65
Operating Pressure (kPa)	101
GDL Compression Ratio (%)	75

2.2.1 Polarization curve response

Despite of ambiguity of the response which only portraits the voltage response at constant current, measurement of I-V curve is a powerful tool that has numerous benefits. First, I-V experiment can be conducted in realistic stoichiometry ratio condition and active area. Mass flow controller connected to customized code response to the current change and provides the exact amount of mass flow of gases.

Therefore, constant current mode is utilized from OCV to 60A. We had experimental sample (JNT30 A6L) that cell operation failed before 60A, however rest of the samples were able to reach 60A performance, and they successfully demonstrate concentration loss region of the cell performance. We tried to make high-load condition that water generation takes a critical role, so relative humidity is controlled to be 100%.

Table 2.4 experimental condition used in polarization curve measurement

Parameter	Condition
Mode	CC Mode (0A → 60A)
Stoichiometry Ratio	1.5/2.0 (Anode/Cathode)
Relative Humidity (%)	100

2.2.2 Electrochemical Impedance Spectroscopy analysis

2.2.2.1 Experimental condition

Table 2.5 Experimental conditions of EIS experiment

Parameter	Condition
Frequency	20KHz to 1Hz
Swing width of AC current	Value between 1.5 and 5% (within a voltage amp. less than 10mV)
Mass flow rate (LPM)	Cathode: 0.64 (SR>10) Anode: 0.2 (SR>10)
Relative Humidity	100%

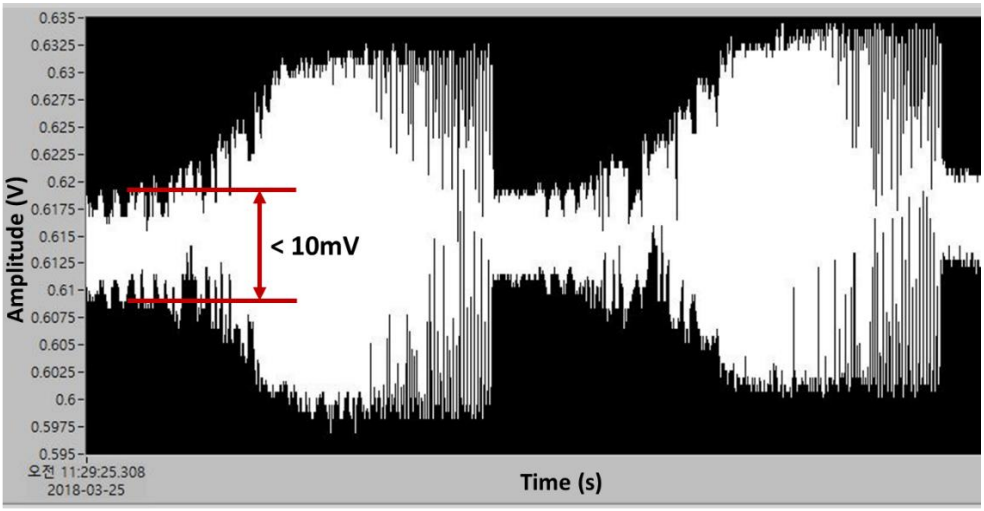

Figure 2.4 Voltage Sensing within 10mV

2.2.2.2 Impedance model analysis (EIS)

At the specific current density region, sinusoidal voltage perturbation within 10mV response as a resultant sinusoidal current response [4]. Impedance response at current density from 0.4 to 2.4 A/cm2 is measured. Swing current is limited from 1.5% to 5% to measure voltage swing response less than 10mV [33, 34]. Active area is limited to 1cm2 close to channel outlet to prevent distribution of oxygen concentration and unwanted flooding phenomenon.

As previous EIS studies has confirmed, [24,25,29,35] proton transport resistance at the catalyst layer led to 45-degree straight line. Once proton transport resistance in cathode develops with the straight line, Resistance regarding oxygen reduction rate develops in semi-circle shape. Figure 2.5 reports the raw impedance data with the fitting model. 45-degree straight line describing the proton transport resistance is observed at high frequency region right after electrical resistance caused from Ohm's law. Resistance caused from oxygen reduction rate (R_orr) can be calculated with bode plot where imaginary impedance region is at peak as measured in Figure 2.6.

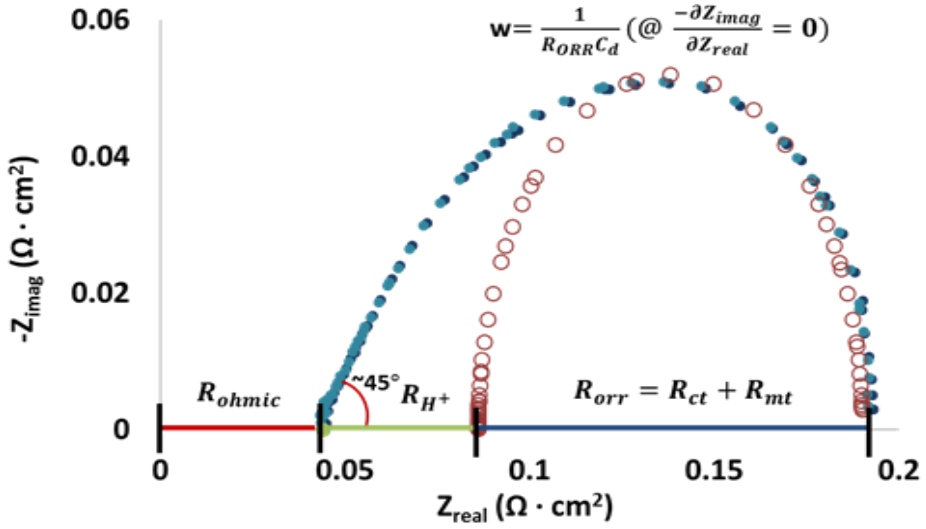

Figure 2.5 Experimental and model impedance data

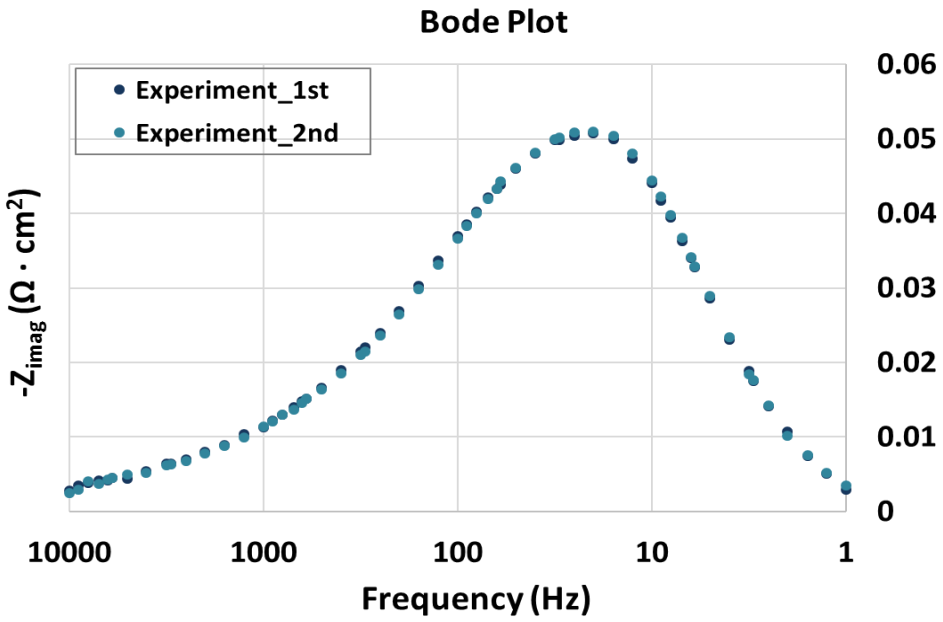

Figure 2.6 Bode plot in EIS experimental result

2.2.2.3 Separation of the activation voltage loss source

Kinetic voltage loss is caused from the characteristics of the membrane-electrolyte assembly. Kinetic voltage loss must be equal among GDL samples. Equation 2.6 gives information that activation over voltage can be extracted from the slope of the modified Butler-Volmer equation [24]. Thus, low current response was measured to extract voltage loss source caused from membrane assembly.

$$i = i_0 \cdot A_{pt} \cdot (\frac{C_{O_2}}{C^*_{O_2}}) exp(\frac{4\alpha F}{RT}\eta_{ORR}) \tag{2.3}$$

$$R_f = \frac{d\eta_{ORR}}{di} = \frac{RT}{4\alpha F}\left[\frac{1}{i} - \frac{1}{i_0}\frac{di_0}{di} - \frac{1}{A_{pt}}\frac{dA_{pt}}{di} - \frac{1}{C_{O_2}}\frac{dC_{O_2}}{di}\right] \tag{2.4}$$

$$R_{ct} = \frac{RT}{4\alpha F} \cdot \frac{1}{i} \tag{2.5}$$

From the slope extracted in low current response in figure 2.7, charge transfer characteristic is calculated as it is inversely proportional to the current. Figure 2.8 portraits the charge transfer resistance in respect of current densities.

$$\eta_{act} = \frac{RT}{4\alpha F}\ln(j_0) + \frac{RT}{\alpha nF}\ln(j) \tag{2.6}$$

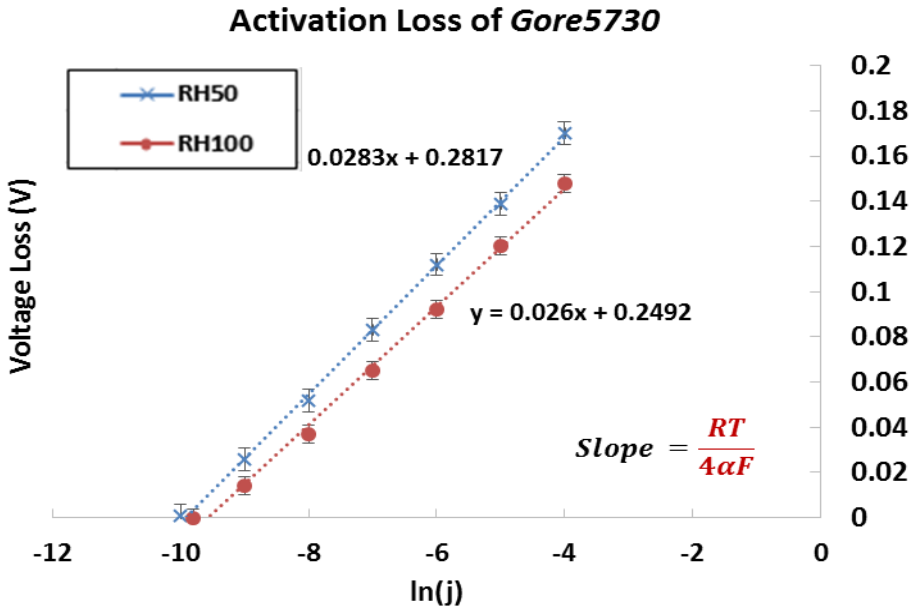

Figure 2.7 Tafel slope of Gore 5730

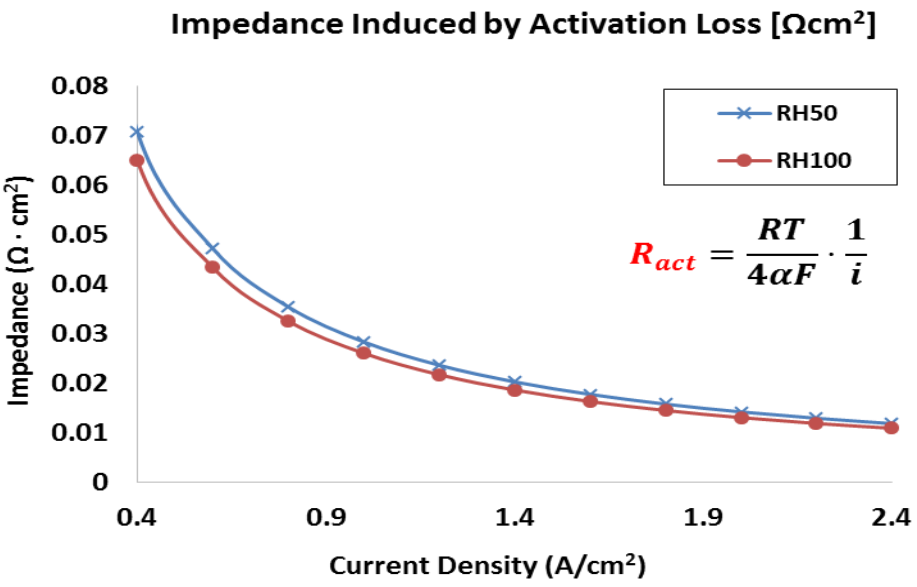

Figure 2.8 Activation voltage loss of Gore 5730

2.2.3 Measurement of the oxygen transport resistance [s/m]

2.2.3.1 Experimental condition

Table 2.6 Limiting current density experimental conditions

Parameter	Condition
Mode	CV Mode (OCV → 0.05V)
Oxygen Concentration	2% (98% with inert gas)
Mass flow rate (LPM)	Cathode: 2.59 (SR>10)
	Anode: 0.2 (SR>10)
Types of Inert Gas	N2, He
Relative Humidity (%)	60~100

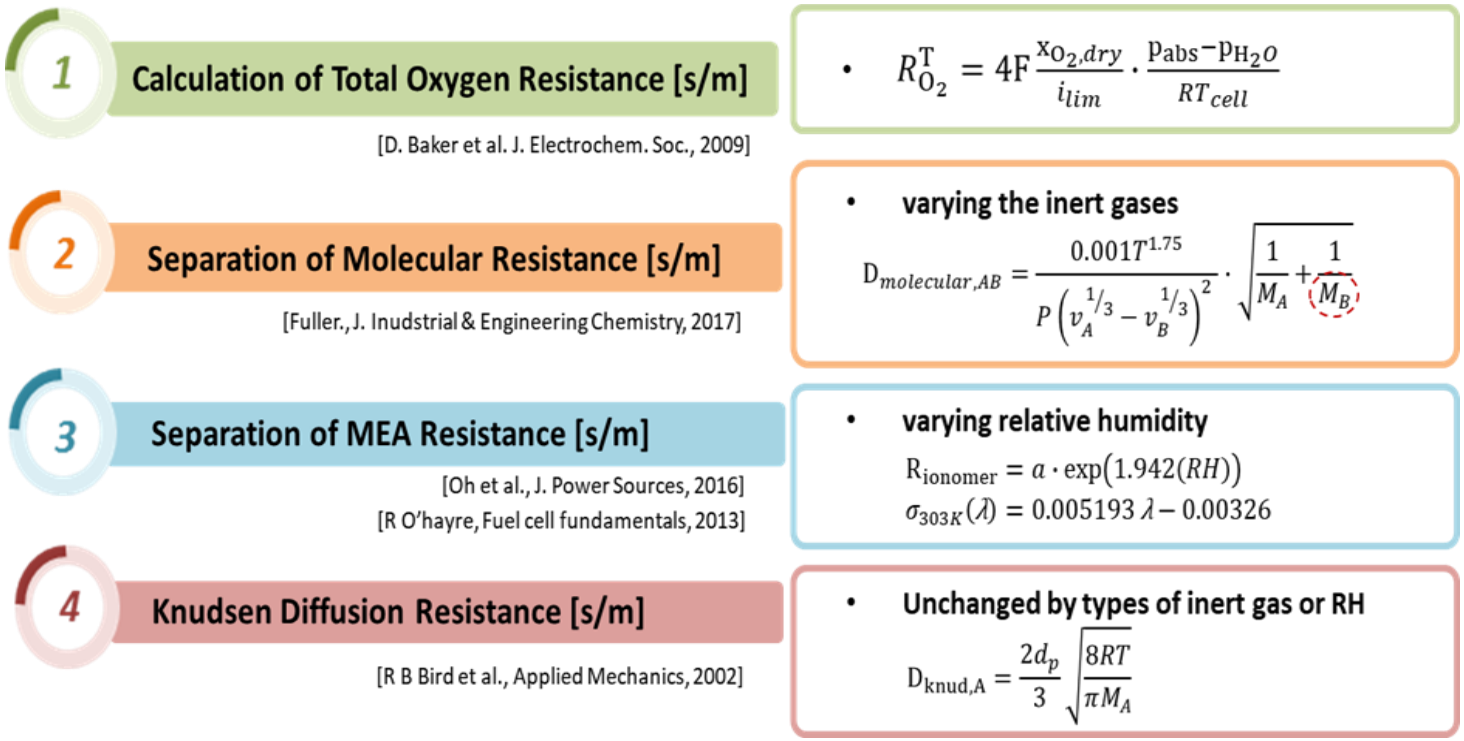

Figure 2.9 Chronological Methodology of LCD analysis

2.2.3.2 Analysis on limiting current density methodology

Oxygen transportation resistance (s/m) is measured to compare the oxygen transporting capability among samples. Measurement of limiting current density was carried out in no water condensation condition. Based on equation characteristics (equation 2.7), total oxygen transportation resistance is calculated and divided into molecular diffusion and Knudsen diffusion and to other resistance caused by catalyst-membrane assembly. Limiting current density method was only applied to compare A3 and A6 samples because the changing ohmic resistant property affects limiting current response and makes it impossible to compare only the transportation ability. Fick's law of diffusion and Faraday's law is applied to calculate the oxygen resistance.

$$R_{O_2}^{T} = 4F\frac{x_{O_2,dry}}{i_{lim}} \cdot \frac{p_{abs} - p_{H_2O}}{RT_{cell}} \tag{2.7}$$

(1) Calculation of total oxygen transport resistance

To make equation 2.7 correct, several assumptions must be satisfied. At limiting current density, oxygen concentration at the catalyst layer is zero due to the calculation assumption that oxygen transport rate (Fick's law) is equal to the oxygen consumption rate (Faraday's' law). Next, Steady-state condition with no water condensation must be achieved. Oh et al. experimentally proved that a cell operation is at steady state when oxygen concentration is limited to 2%.

(2) Separation of molecular diffusion resistance

As appears in table 2.7, molecular diffusion coefficient is affected by Temperature, Pressure, diffusion volume, and molar mass of molecules to collide. In this study, molar mass of the inert gas is controlled with helium and nitrogen to separate the molecular diffusion. To calculate the diffusion coefficient of molecular diffusion, diffusion volume was referenced from work of Perry [31].

$$\frac{\mathrm{R}^{\mathrm{MD}}_{O_2-N_2}}{\mathrm{R}^{\mathrm{MD}}_{O_2-He}} = \frac{\mathrm{D}^{\mathrm{MD}}_{O_2-He}}{\mathrm{D}^{\mathrm{MD}}_{O_2-N_2}} \tag{2.8}$$

$$\mathrm{R}^{\mathrm{T}}_{O_2-N_2} - \mathrm{R}^{\mathrm{MD}}_{O_2-N_2} = \mathrm{R}^{\mathrm{T}}_{O_2-He} - \mathrm{R}^{\mathrm{MD}}_{O_2-He} \tag{2.9}$$

(3) Separation of MEA transporting resistance

Separation of oxygen transport resistance at MEA is performed by varying the relative humidity. There are two mechanisms occurring in membrane-electrolyte assembly which affect the oxygen transport resistance. First, ionic conductivity of electrolyte affects the limiting current density response [32]. Although it does not in terms of oxygen transport resistance (s/m), poor ionic conductivity worsens the oxygen reduction occurring at the cathode side and makes concentration consumption slow. As relative humidity increases, ionic conductivity increase proportionally enhancing the oxygen reduction rate. Oxygen permeation through Ionomer film directly affects the oxygen transportation. Table 3.5 contains the equation regarding ionomer permeation. However, due to the ionic conductivity characteristic that will proportionally affect the limiting current density response, oxygen transport resistance caused in MEA has to contain the coefficient that covers enhancing current response due to the relative humidity increase.

$$\mathrm{R}_{MEA} = a \cdot \exp\big(b \cdot (RH)\big) \tag{2.10}$$

(4) Prediction model of air injection to the cathode

We can predict the oxygen transport response when actual air content is applied to the cathode by using the given parameters in table 6. First, mole fraction of the gas phase water is calculated at each operated relative humidity; with our experimental conditions of atmospheric pressure and 65-degree Celsius, partial pressure of water content of corresponding relative humidity calculated and then calculated into mole fraction. 20.946 Mole% of oxygen among air is then recalculated with the vapor water fraction.

$$\mathrm{R}_{\mathrm{Air}}^{\mathrm{MD}} = \frac{\mathrm{R}_{O_2-He}^{\mathrm{MD}}}{\mathrm{R}_{\mathrm{Air}}^{\mathrm{MD}}} \cdot \mathrm{R}_{O_2-He}^{\mathrm{MD}} \tag{2.11}$$

Table 2.7 Equations regarding the oxygen transport resistance

Ref.	Nom	Equation
[36]	Molecular diffusion Coefficient	$\mathrm{D}_{AB} = \frac{0.001T^{1.75}}{P\left(v_A^{1/3} - v_B^{1/3}\right)^2} \cdot \sqrt{\frac{1}{M_A} + \frac{1}{M_B}}$
[24]	Ionic Conductivity	$\sigma_{303K}(\lambda) = 0.005193\,\lambda - 0.00326$
[5]	Ionomer Permeation	$\mathrm{R}_{\mathrm{ionomer}} = a \cdot \exp\big(b \cdot (RH)\big)$
[37]	Knudsen Diffusion Coefficient	$\mathrm{D}_{\mathrm{knud,A}} = \frac{2d_p}{3}\sqrt{\frac{8RT}{\pi M_A}}$

Chapter 3. Material Properties of MPL Samples

3.1 Measurement of pore size diameter in MPL

Measurement of MPL porosity was utilized by mercury intrusion porosimetry. Intrusion of non-wetting fluid (mercury) through a porous media can only be initiated by an external pressure, and higher pressure for intrusion is required as pore size diameter gets smaller [38]. Based on the theory, we could measure the pore size diameter of MPL and GDBL. Examination of Mercury intrusion porosimetry is conducted with Auto Pore V of Micrometics Company.

3.1.1 Compression test

Before measuring the pore size diameter of MPL, we experimented how the compression torque affects GDL pore properties. In Figure 3.1, two responses of GDL pore size response are explicated with raw GDL and one with the compression force applied. Left peak of the graph portraits the MPL pore size diameter, and right one shows pore size of GDBL side. Exam was conducted with JNT30-A3 with thickness of 310um. Extreme condition was applied when the compression torque was applied; we assured that GDL goes through the permanent deformation to the thickness of the gasket which we targeted to be 80% of the original GDL thickness. Nonetheless, it is confident that MPL pore size diameter was not affected. Not only MPL pore size was unchanged, but also GDBL maintained its peak average diameter.

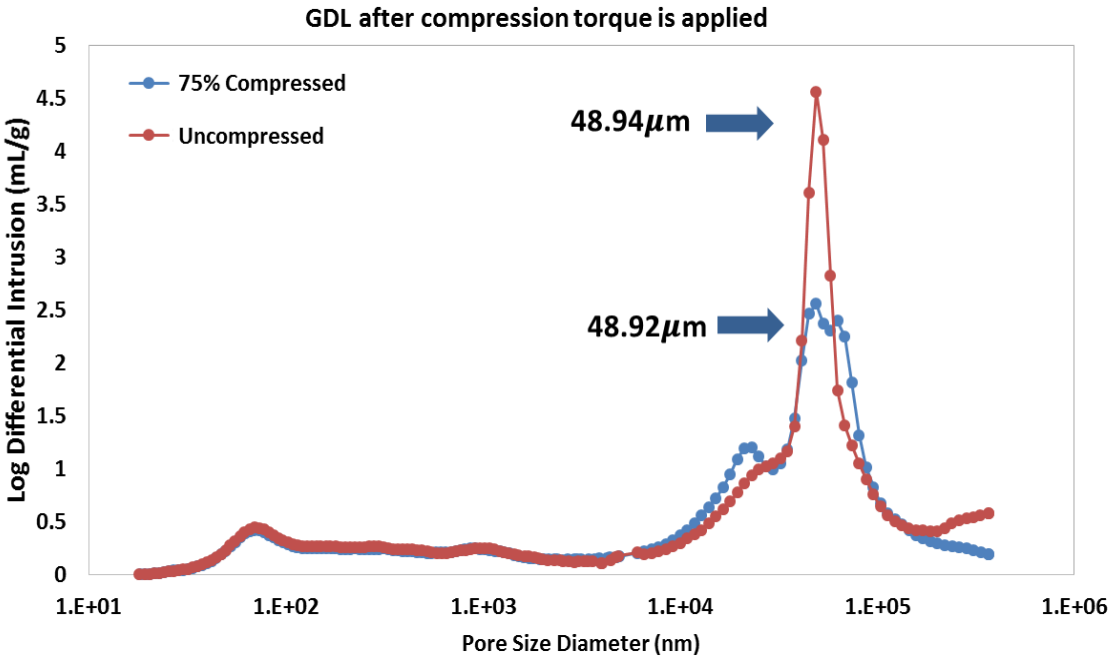

Figure 3.1 GDL porosimetry after compression torque is applied

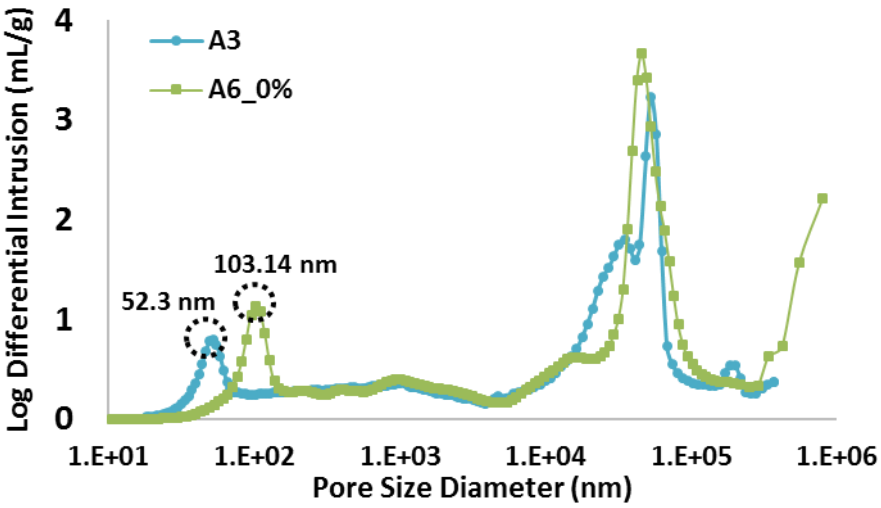

(a)

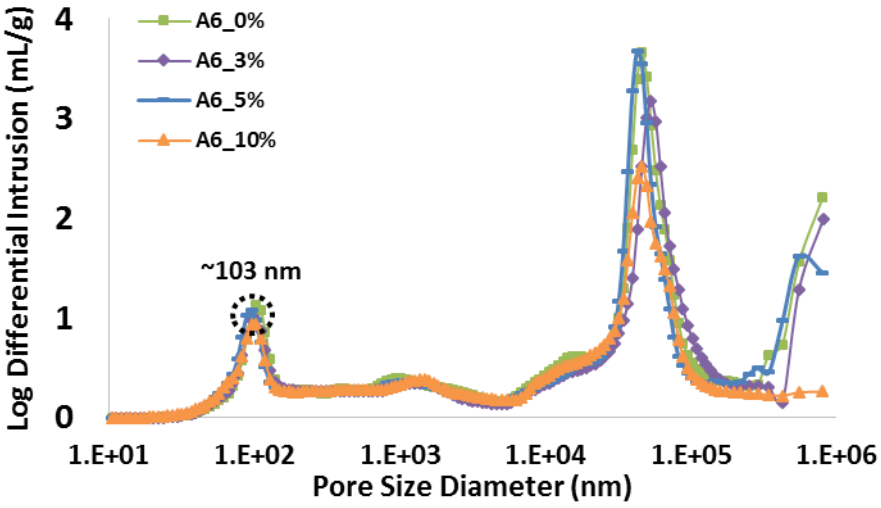

(b)

Figure 3.2 Porosimetry measurement of experimental samples

3.1.2 Pore size diameter of experimental samples

Figure 3.2 demonstrates a graph of log differential intrusion versus pore size diameter of experimental samples. Left peak of the intrusion depicts the pore size diameter of MPL. As targeted, pore size diameter of Sample A3 and A6 converges in the order of 50nm and 100nm. Also, in figure 2.3, A6 series with varied carbon black content, targeted pore size diameter all converges within 0.03% error.

Identical GDBL is applied to all the MPL samples, all the GDBL pore sizes converge close to 50 microns.

3.2 Measurement of MPL surface contact angle

Contact angle is measured in home-made contact angle meter. Schematic of the test device is portrayed in Figure 3.3. 10uL of water droplet was carefully dropped on the surface of MPL by using micro syringe. Horizontality of the samples is assured to be horizontal. Image processing and analysis of contact angle is conducted three times to make sure the repeatability of sample contact angle.

Contact angle of each experimental samples is shown in figure 3.4 after their repeatability being assured. Carbon A3 and A6, regardless of their difference in particle sizes, portrayed the identical contact angle. However, difference in contact angle is observed in samples where carbon type C was added. MPL with C type carbon content increased contact angle as the weight percent arises.

Although, the result does not directly provides the index of certain material characteristics, this phenomenon signifies the possibility of the increasing hydrophilic property. With measurement of the contact angle, it was expected that Carbon C content may influence in poor water management ability.

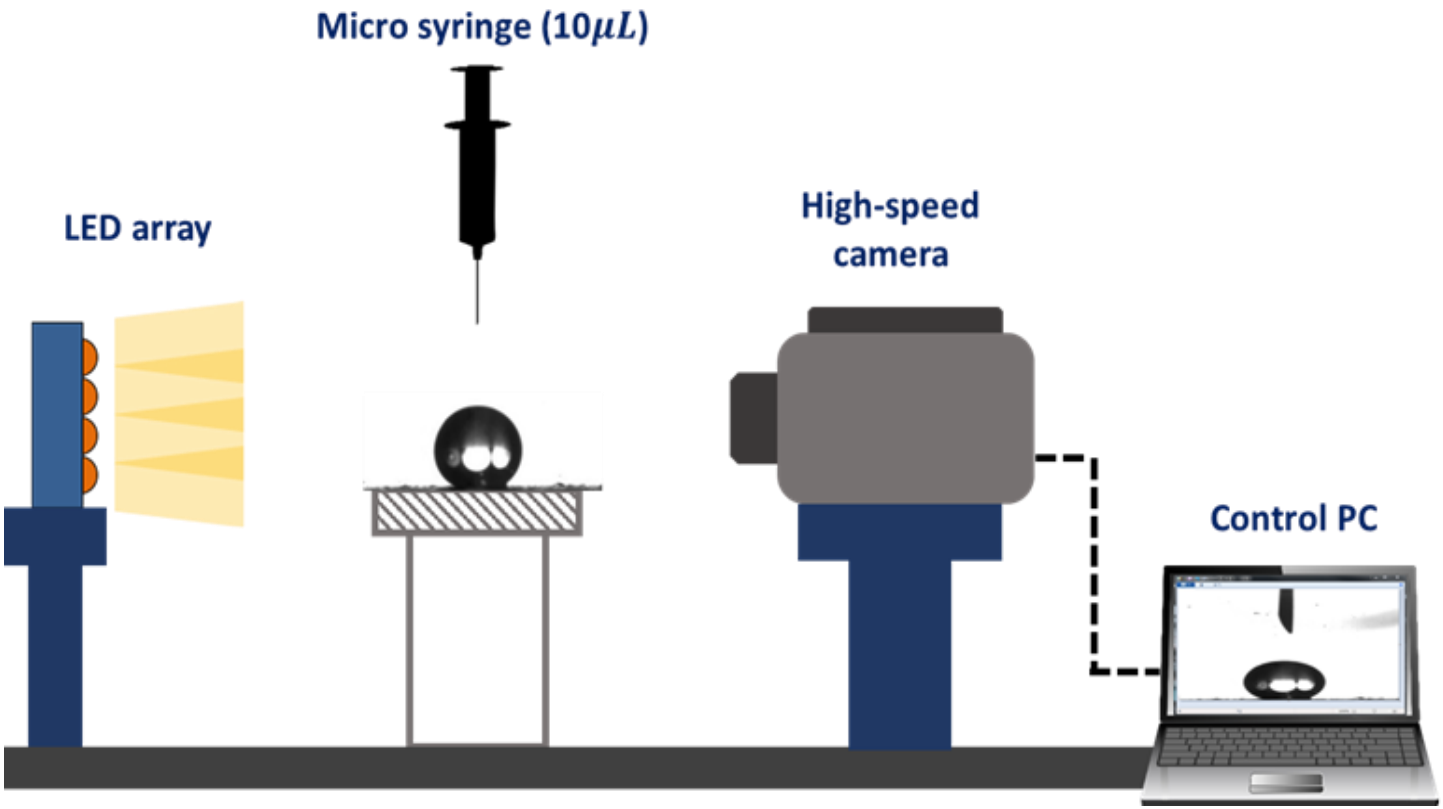

Figure 3.3 Schematic of contact angle meter of water droplet

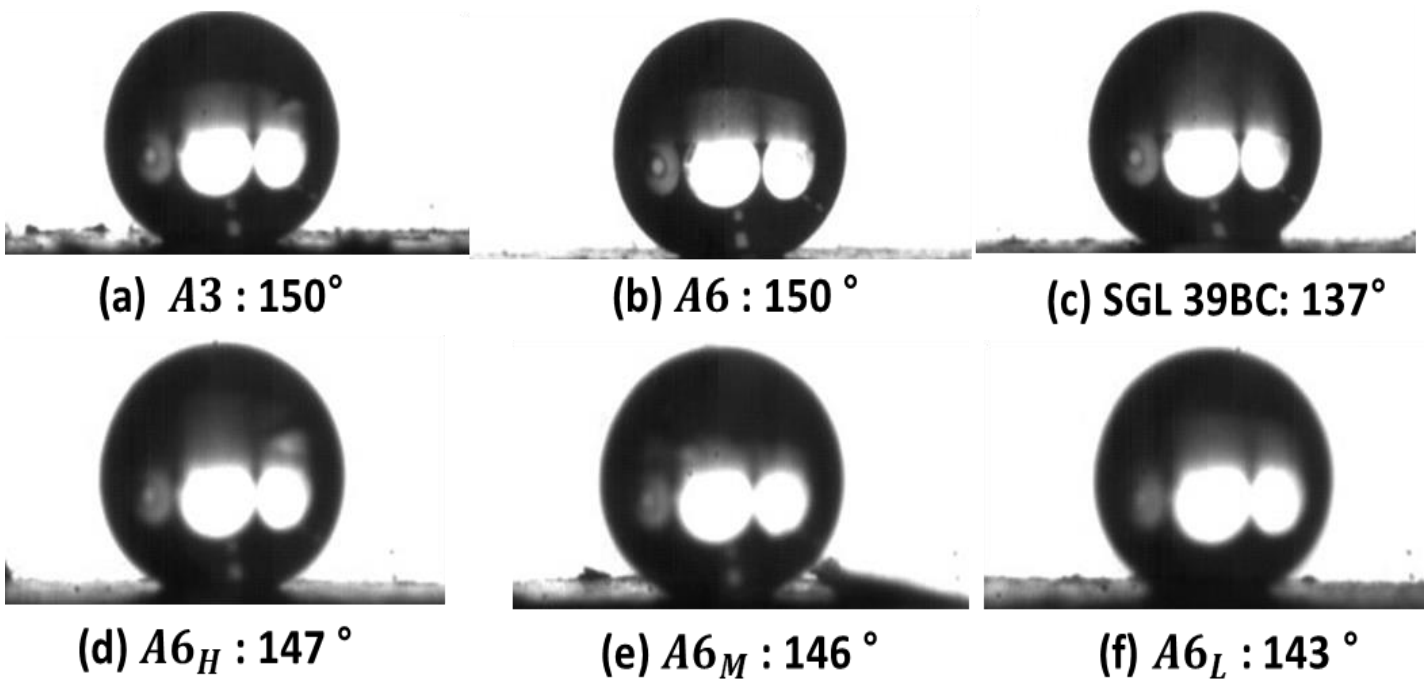

Figure 3.4 Image analysis of droplet on MPL surfaces

3.3 Element property of MPL surface

Scanning Electron Microscope (SEM) is utilized to grasp the characteristics of MPL surface and to assure there is no malfunctions on experimental GDL samples.

We conducted the image processing and material analysis to visually and analytically compare GDL characteristics. First, material analysis is utilized at the MPL surface at 1k magnification. Electrons are scattered to the surface of the MPL. Each electrons response as resolution of certain era and provide elemental properties [39]. All samples of various points of detection. We measured that fluorine weight distribution varied from 26.45% to 28.84%. Fluorine content was result of PTFE content of MPL. Identical fluorine content on MPL surfaces proves the negligible differences in PTFE treatment among MPL samples. In result, we could conclude that following differences in contact angle with water droplet of samples are not attributed from PTFE contents.

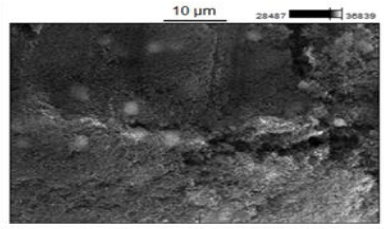

Element	Weight %	Atom %
C K	66.16	75.06
O K	5.00	4.26
F K	28.84	20.69
Total	100.00	100.00

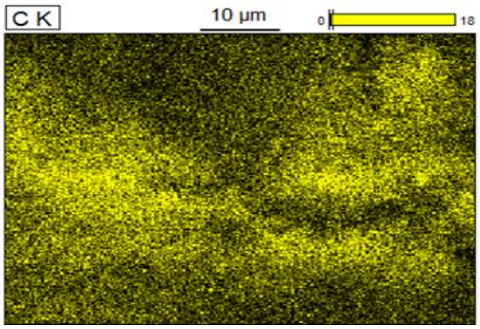

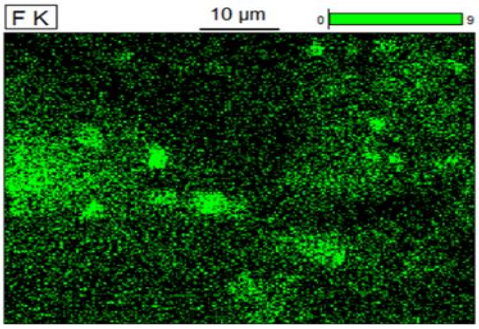

Figure 3.5 SEM: material analysis

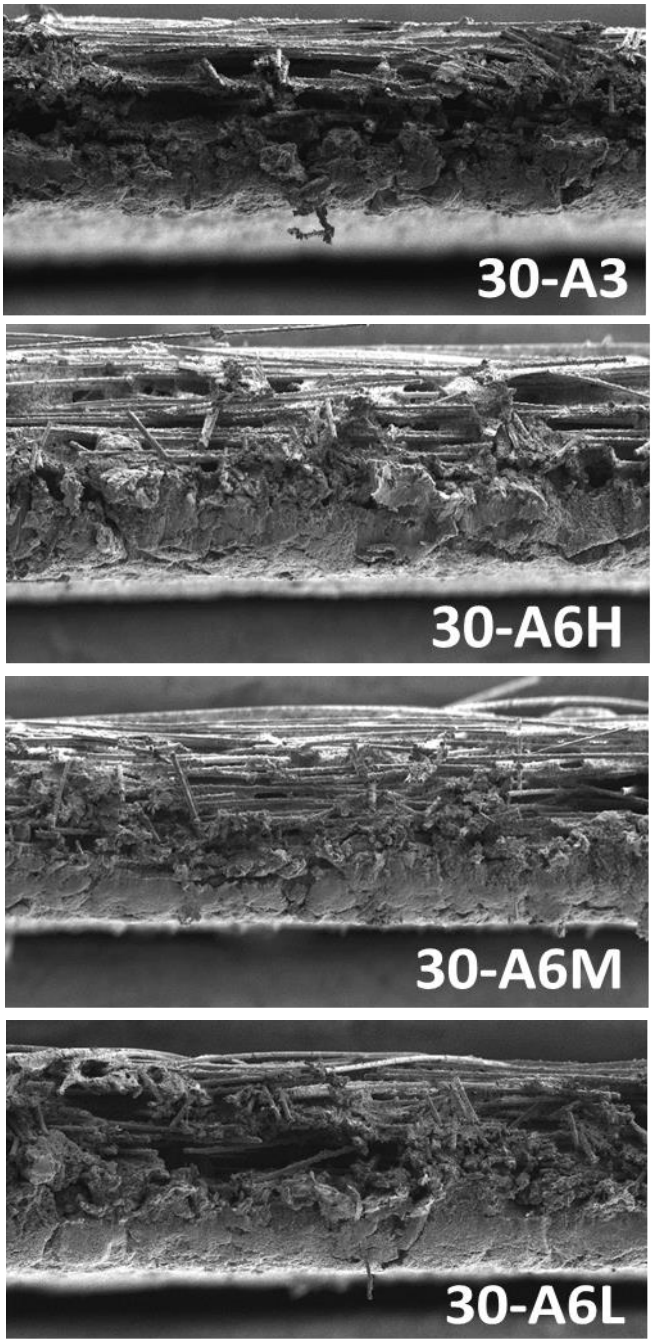

Figure 3.6 cross-sectional SEM image of GDL samples

Chapter 4. Experimental Results

4.1 Experimental results of pore size- graded samples

4.1.1 Polarization curve response

Activation loss region must be identical for both A3 and A6 MPL samples. In fact, this phenomenon was also expected before the experiment because activation loss is predominant in early stage of the cell operation and is majorly affected by the type of catalyst layer. In a low current density region, the concentration on the surface of the catalyst layer isn't fully depleted. So the early stage response must converge in similar shape as it is for the experimental result.

Ohmic loss is proportional to the current density and the experimental result of A3 vs. A6 also depicted the similar ohmic loss response. Carbon powder A3 and A6 have identical electrical conductivity, so identical ohmic property is portrayed in polarization curve as well.

In polarization response, concentration loss region performance enhancement is portrayed. Concentration over voltage influences the fuel cell performance of A3 sample and initiating the concentration loss at 1.4 A/cm2. Power density of A6 peaked to be 0.936W/cm2 at 1.9A/cm2 while that of A3 maxed to be 0.866 W/cm2 at 1.7A/cm2. Thus, I-V curve informs a general information of power density and corresponding current density that power had peaked. Total power density increment was 8% for twice larger pore size diameter.

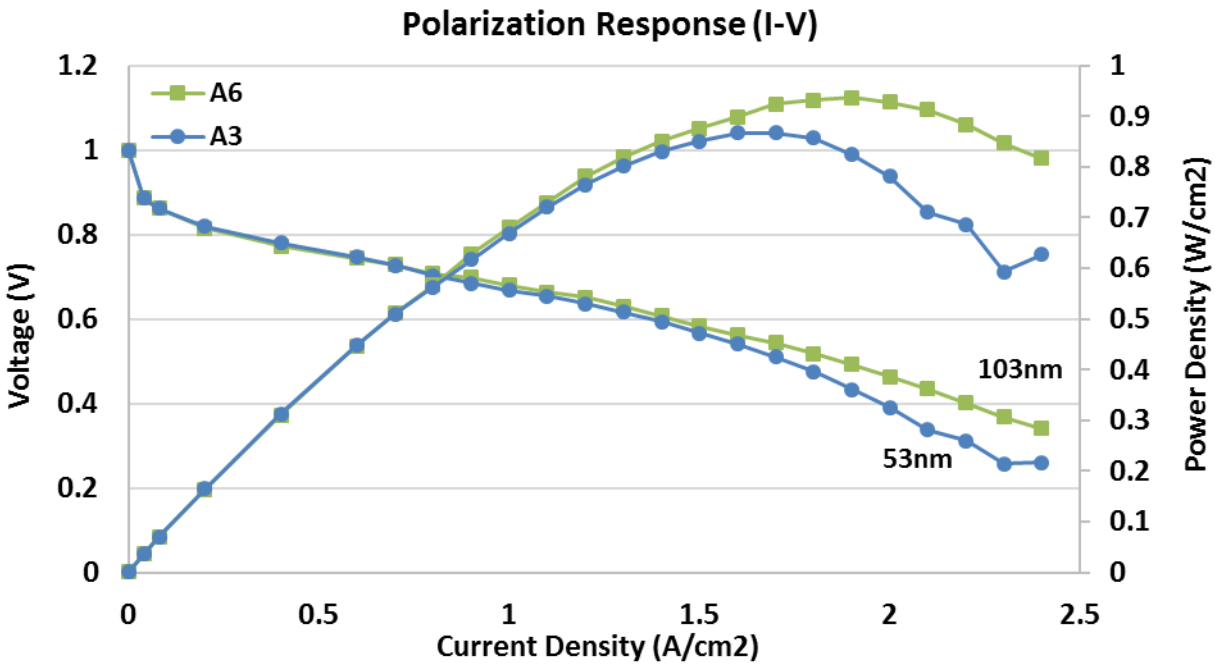

Figure 4.1 Polarization curve of A3 vs. A6

4.1.2 Result of EIS model analysis

Resistances of activation, ohmic, and concentration loss are separated by utilizing EIS technique. Activation loss portion is already portrayed in previous chapter, so only the ohmic and concentration region of voltage loss are investigated in this section.

Identical ohmic resistance characteristic of A3 and A6 appears in figure. 4.2. Figure 4.2 depicts the concentration over voltage. It can be observed that the trend with A3 sample initiates concentration loss at 1.4A/cm2 and severely drops its voltage. If we recall the ohmic property portrayed in the polarization response, such ohmic characteristic is reasonable. Both A3 and A6 converged around 0.093 ohm cm2.

Concentration voltage loss portion had the identical trend as the polarization curve response. We recall that peak current density of A3 was 1.4 A/cm2. In the EIS response of different active area, severe concentration loss begins at 1.4 A/cm2 as well. Such response is conducted in highly humidified conditions. Therefore, we could not conclude that such concentration loss response is caused from enhanced capillary action or for the oxygen transportation. So in this section we assure that EIS response of concentration was identical with the polarization response and move on to the limiting current density response.

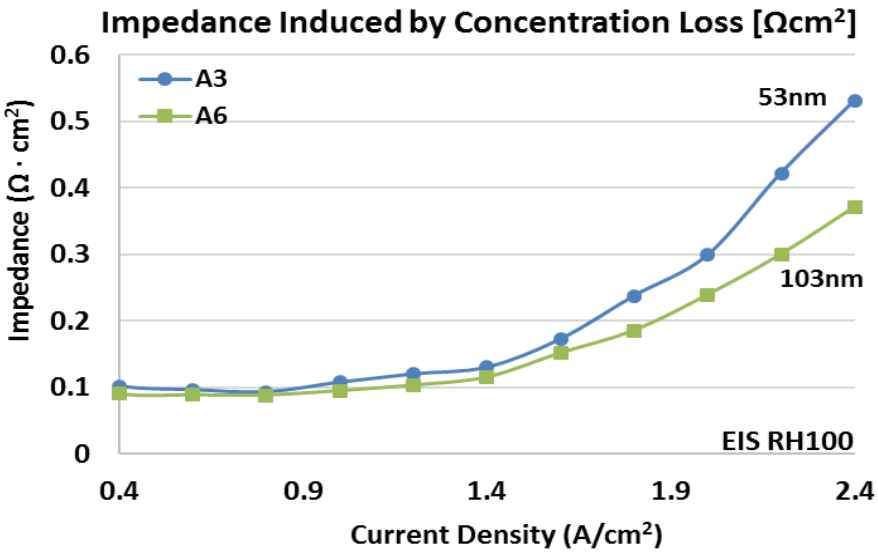

Figure 4.2 Concentration voltage loss: A3 vs. A6

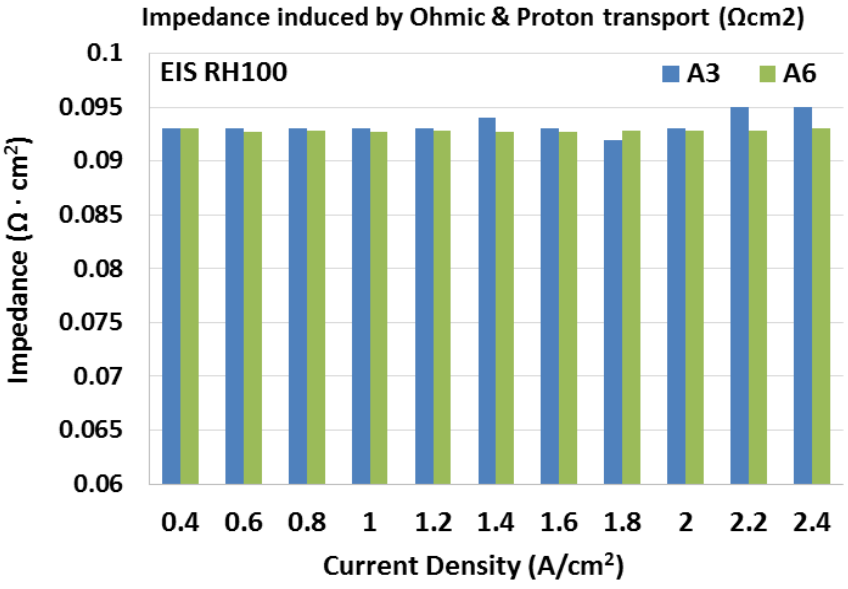

Figure 4.3 Ohmic & Proton transport voltage loss: A3 vs. A6

4.1.3 Measurement of oxygen transport resistance [s/m]

Identical trend of concentration losses is observed in both I-V and EIS responses, yet it is hard to conclude which criteria is enhanced whether if it is water removing ability or the oxygen transportation mechanism. Thus, limiting current density response is measured to analyze only the oxygen transportation capacity.

Figure 4.4 is the result of analyzed limiting current density response. Each oxygen transportation losses are quantitatively separated into resistance caused by molecular, Knudsen diffusion and MEA. Experimental results of various relative humidity are depicted in the figure and mostly we'd like to focus on relative 100% condition.

In low relative humidity condition, oxygen transportation of MPL of smaller pore size diameter (A3) rather superior. This is because in low humidified condition, hydrophilic property is beneficial to operate a fuel cell to maintain membrane humidity rather than removing vaporized water out of the system.

For larger pore size diameter (A6), resistance caused by Knudsen diffusion decreases, but that of molecular diffusion rises. From the limiting current density result, we can see that the total oxygen transport resistance values all in identical range of error bar. In other words, larger pore size diameter barely affects the oxygen transportation but does enhance the water removal capability.

Based on the polarization curve, EIS result on concentration loss portion and limiting current density response, we revealed the major concentration loss enhancement by larger pore size diameter was by its enhanced capillary action.

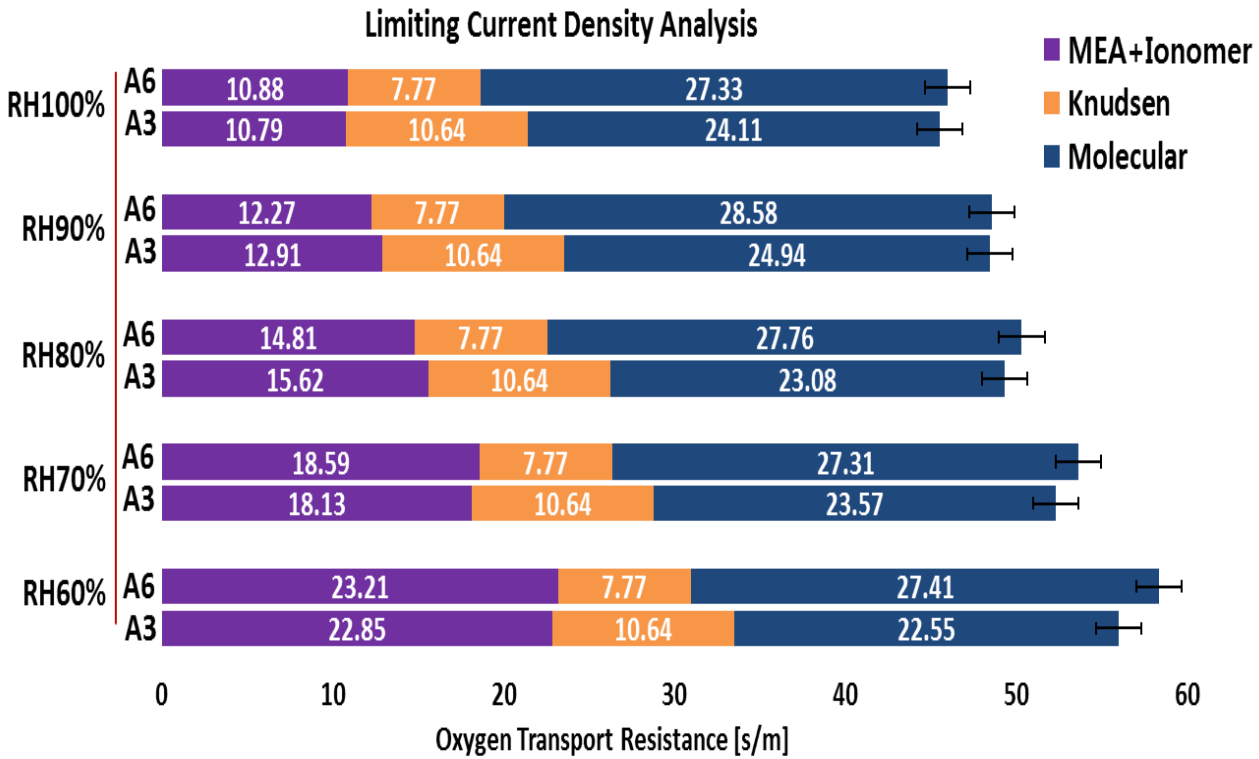

Figure 4.4 LCD results: A3 vs. A6

4.2 Experimental results of conductive additives

4.2.1 Polarization curve response

Figure 4.5 depicts the results of experimental samples that carbon C content is gradually added. As written in table 4.1, we can conclude that concentration loss region worsens with the carbon content increment with the fact that peak current density is being advanced. Despite of performance increment due to ohmic property enhancement, peak current density was maximum at 1.9 A/cm2 for A6 with no conductive additive. When 3 wt. % and 5 wt. % of carbon C were utilized, peak current density advances as 1.8 A/cm2, and when 10 wt. % of carbon C content was applied, we can see that concentration loss dramatically increases and initiates comparatively early stage of operation. Despite of the early initiation of the concentration loss of all cases, peak power density of cell. Increment of the power density is not significantly but consistent.

Table 4.1 Peak current density and power density of conductive additives

Case	**Peak j [A/cm^2]**	**Peak power [W/cm^2]**
A6	1.9	0.936
A6H	1.8	0.977
A6M	1.8	0.972
A6L	1.5	0.815

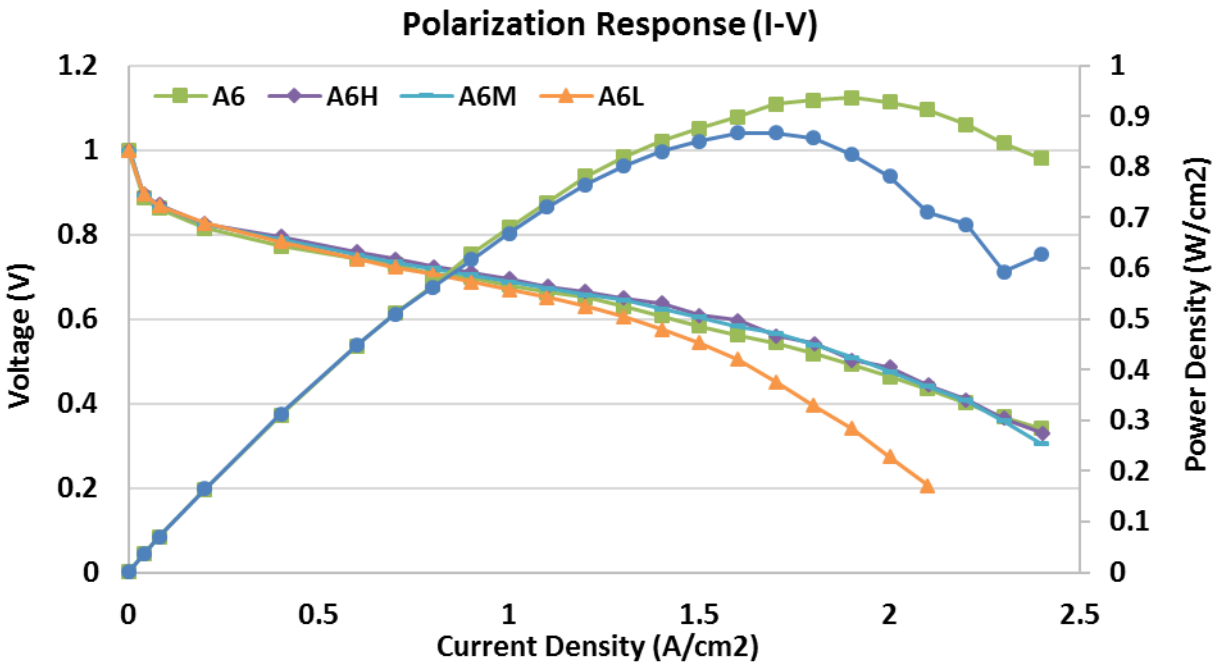

Figure 4.5 Polarization response A6 with conductive additives

4.2.2 Result of EIS model analysis

In polarization response, slightly decreasing concentration loss was revealed, and enhanced ohmic property was also revealed with the fact that peak power density increased regardless of peak current density is being advanced. With EIS analysis, we were able to quantitatively separate ohmic and concentration overvoltage portion of the performance response.

When conductive carbon type C was gradually added, ohmic characteristics also proportionally increased. A6 had similar ohmic characteristics as A3 sample as we already have discussed. 3 wt. % of C type to 10 wt. %, gradual decrement of ohmic resistance is portrayed in figure 4.7. More than 10% of ohmic property enhanced with 10 wt. % of additives.

However, when 10 wt. % of conductive additive was applied, severe flooding caused concentration loss initiation. It started comparatively early stage of current density of 1.3A/cm^2. A6H and A6M also initiated the concentration voltage loss comparatively early.

We revealed the trade-off relationship when conductive additives are applied to the single carbon content. It advances the initiation of the concentration loss, but small amount of conductive additive rather increased the peak power density, and it was concluded to be helpful for the cell performance increment.

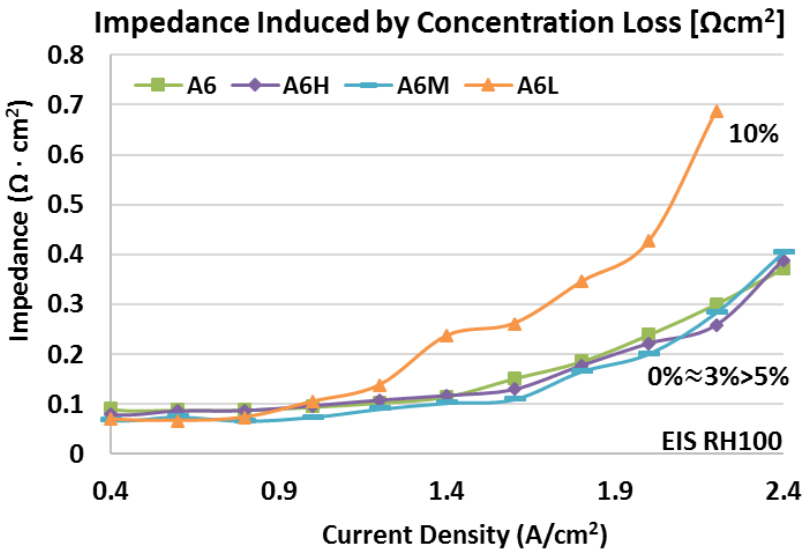

Figure 4.6 Concentration voltage loss of conductive additives

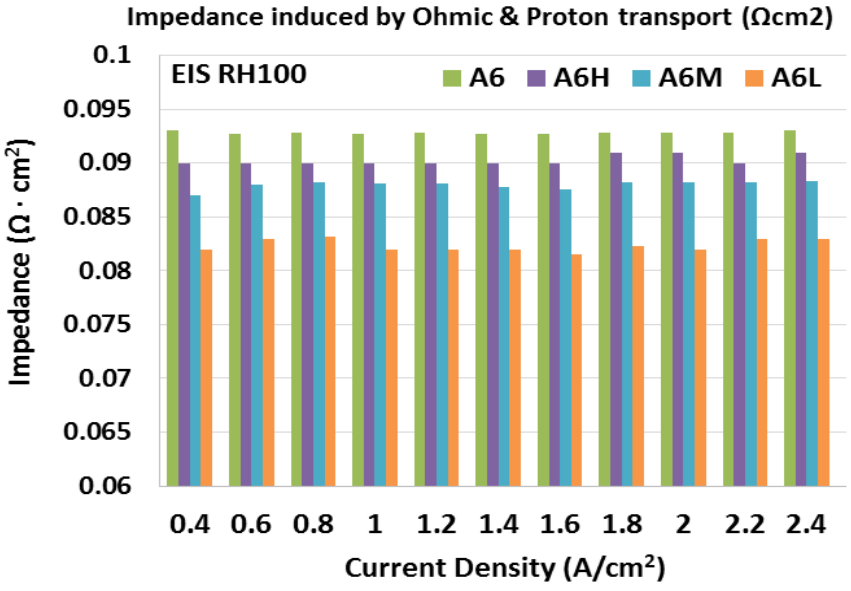

Figure 4.7 Ohmic & Proton transport loss of conductive additives

4.3 Overall results

Overall performances among experimental samples are compared. We have conducted 3 different experiments to reveal causes of such experimental results. When a larger pore size diameter is utilized in MPL, capillary pressure is reduced and reduces the concentration voltage loss region. And when a conductive additive is gradually applied in the MPL slurry, ohmic loss is reduced and increased the performance despite of the advanced initiation of the concentration loss.

Based on the fact EIS analysis, we successfully separated total voltage loss of response into activation, ohmic and concentration loss. Also, they are compared into 4 operation points: Extremely low current density (0.4A/cm2), Medium current density (1.2 A/cm2), High current density (1.8 A/cm2), and extremely high current density (2.2 A/cm2).

In an extremely low current density, activation voltage loss is dominant. Activation loss itself takes 47% of whole voltage losses. Activation loss, then exponentially decrease and become negligible at high current density region.

Ohmic voltage loss is linearly proportional to the current density. It cannot be negligible from all regions of the cell operation but becomes only more important towards medium and high current density region.

Concentration loss becomes dominant from high current density region and severely increase at extremely high current density region. In case of A6, 77% of total voltage loss is taken from the concentration loss region.

Among experimental samples, A6L portrayed the worst performance at all current density region and A6H portrayed the best performance which is 9% enhanced compared to the commercial sample (A3).

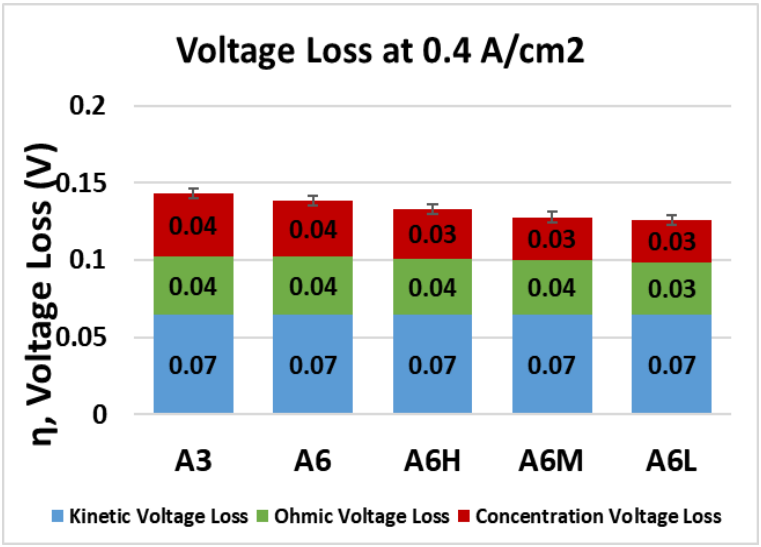

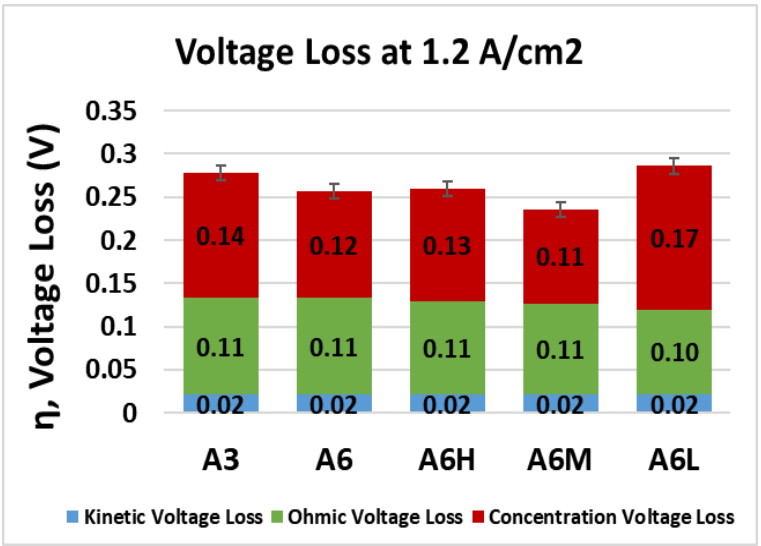

Figure 4.8 Sources of voltage loss at low current densities

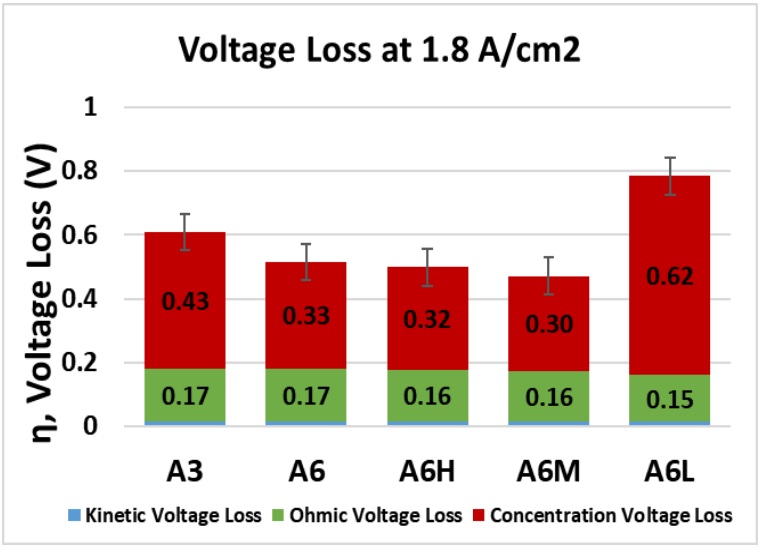

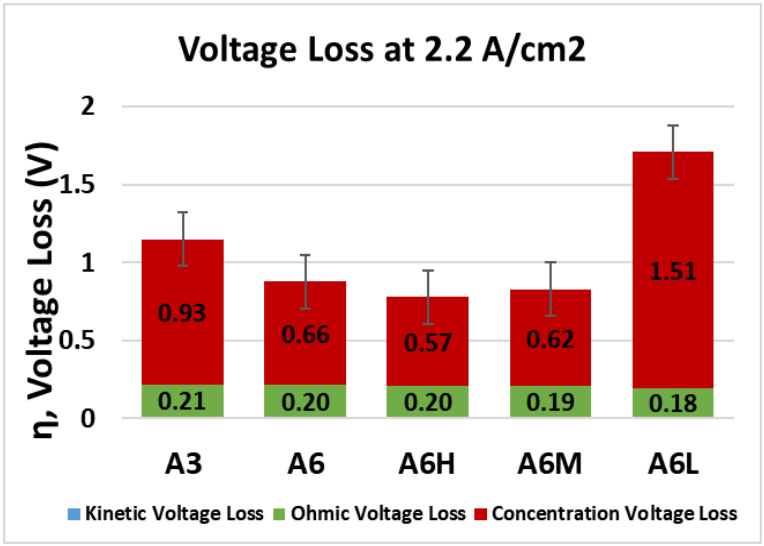

Figure 4.9 Sources of voltage loss at high current densities

Chapter 5. Conclusion

Under current technological progresses that fuel cell researchers have achieved, a modern design index for gas diffusion layer was required. Therefore, MPL material properties are varied to optimize the fuel cell performance.

First, MPL pore size diameter was varied from 52nm (A3) to 103nm (A6). Concentration over voltage region reformed as MPL pore diameter increased to 103nm. In no water condensation condition, resistance of Knudsen diffusion decreased, but molecular diffusion increased. The total oxygen transportation resistance Same trend was depicted in Electrochemical Impedance Spectroscopy results. In Sample A3, Severe flooding caused the blockage of the oxygen transportation from 1.6A/cm2 at Sample A3. On the other hand, A6 with 103nm pore size diameter improved the capability of removing excessive by-product and ameliorated overvoltage by 0.36V at current density 2.4A/cm2.

Carbon black with superior electrical conductivity was gradually added to A6. Conductive carbon additive had a trade-off relation of advancing the concentration loss region while conductivity of the material improves. Therefore, optimal percentage of the additive was to be found where improving the ohmic resistance dominates the advancing concentration over voltage region. Up to 3% of the conductive carbon addition, concentration over voltage was not affected while ohmic conductivity improved. At 5% additives, flooding at high current density causes concentration over voltage, and performance with no additive gets better at 2.4 A/cm2. Up to 10%, cell performance gradually decreases and causes severe concentration voltage loss.

In conclusion, GDL sample with MPL pore diameter of 103nm with 3% content conductive carbon black additives had the best performance among MPL with various material properties.

This study is concluded with a summary in chronological order.

(1) Various MPL material properties are investigated
In this study, various MPL material properties are investigated by manufacturing 5 experimental MPL samples on an identical GDBL. Pore size diameter was graded from 53nm to 103nm. Additionally, conductive carbon powder was added in MPL slurry from 0 to 10 wt.%.

(2) Enlarged pore sized MPL enhanced the concentration voltage loss region.
We observed the enhancement of the concentration loss region by enlarging the pore size diameter. By limiting current density response, it was revealed that oxygen transportation isn't enhanced by increment of pore size diameter. Also, the trade-off relation of oxygen transportation behavior of molecular diffusion and Knudsen diffusion is revealed. Increment of the pore size diameter improves the capillary action to reduce the concentration loss region.

(3) Conductive additive improves conductivity but advanced the concentration loss region
Conductive additives reduced ohmic resistance as targeted; however, the tradeoff relationship of applying carbon C was revealed. As ohmic loss region improves, concentration loss region is advanced.

(4) Analytic techniques are confirmed with comparison among samples.
Lastly, advanced analytic techniques such as EIS and limiting current density method were utilized, and they all demonstrated the identical trend of responses. Investigation of quantitative voltage loss and oxygen transportation ability is successfully conducted through the experiments.

Bibliography

[1] C. C. Chan, "The state of the art of electric, hybrid, and fuel cell vehicles," *Proceedings of the IEEE*, vol. 95, no. 4, pp. 704-718, 2007.

[2] K. Kojima and K. Fukazawa, "Current status and future outlook of fuel cell vehicle development in TOYOTA," *ECS Transactions*, vol. 69, no. 17, pp. 213-219, 2015.

[3] T. Suzuki, "Fuel Cell Stack Technology of Toyota," *ECS Transactions*, vol. 75, no. 14, pp. 423-434, 2016.

[4] T. Yoshida and K. Kojima, "Toyota MIRAI fuel cell vehicle and progress toward a future hydrogen society," *The Electrochemical Society Interface*, vol. 24, no. 2, pp. 45-49, 2015.

[5] H. Oh, Y. il Lee *et al.*, "Experimental dissection of oxygen transport resistance in the components of a polymer electrolyte membrane fuel cell," *Journal of Power Sources*, vol. 345, pp. 67-77, 2017.

[6] J. D. Miller and C. Façanha, "The state of clean transport policy: A 2014 synthesis of vehicle and fuel policy developments," 2014.

[7] P. Costamagna and S. Srinivasan, "Quantum jumps in the PEMFC science and technology from the 1960s to the year 2000: Part II. Engineering, technology development and application aspects," *Journal of power sources*, vol. 102, no. 1-2, pp. 253-269, 2001.

[8] V. Mehta and J. S. Cooper, "Review and analysis of PEM fuel cell design and manufacturing," *Journal of Power Sources*, vol. 114, no. 1, pp. 32-53, 2003.

[9] S. Litster, D. Sinton *et al.*, "Ex situ visualization of liquid water transport in PEM fuel cell gas diffusion layers," *Journal of Power Sources,* vol. 154, no. 1, pp. 95-105, 2006.

[10] G. Kolyagin and V. Kornienko, "The effect of carbon black mixture composition on the structural and electrochemical characteristics of gas diffusion electrodes for electrosynthesis of hydrogen peroxide," *Russian Journal of Electrochemistry,* vol. 52, no. 2, pp. 185-191, 2016.

[11] S. Park, J.-W. Lee *et al.*, "A review of gas diffusion layer in PEM fuel cells: materials and designs," *International Journal of Hydrogen Energy,* vol. 37, no. 7, pp. 5850-5865, 2012.

[12] C.-J. Tseng and S.-K. Lo, "Effects of microstructure characteristics of gas diffusion layer and microporous layer on the performance of PEMFC," *Energy conversion and management,* vol. 51, no. 4, pp. 677-684, 2010.

[13] X. Wang, H. Zhang *et al.*, "A bi-functional micro-porous layer with composite carbon black for PEM fuel cells," *Journal of Power Sources,* vol. 162, no. 1, pp. 474-479, 2006.

[14] H. Tang, S. Wang *et al.*, "Porosity-graded micro-porous layers for polymer electrolyte membrane fuel cells," *Journal of power sources,* vol. 166, no. 1, pp. 41-46, 2007.

[15] J. H. Chun, D. H. Jo *et al.*, "Development of a porosity-graded micro porous layer using thermal expandable graphite for proton exchange membrane fuel cells," *Renewable energy,* vol. 58, pp. 28-33, 2013.

[16] T. Tanuma and M. Kawamoto, "Effect of Pore Volume of Hydrophilic Microporous Layer (MPL) on PEFC Performance," *ECS Transactions,* vol. 69, no. 17, pp. 1323-1329, 2015.

[17] C. Simon, D. Kartouzian *et al.*, "Impact of Microporous Layer Pore Properties on Liquid Water Transport in PEM Fuel Cells: Carbon Black Type and Perforation," *Journal of The Electrochemical Society,* vol. 164, no. 14, pp. F1697-F1711, 2017.

[18] D. R. Baker, D. A. Caulk *et al.*, "Measurement of oxygen transport resistance in PEM fuel cells by limiting current methods," *Journal of The Electrochemical Society,* vol. 156, no. 9, pp. B991-B1003, 2009.

[19] N. Nonoyama, S. Okazaki *et al.*, "Analysis of oxygen-transport diffusion resistance in proton-exchange-membrane fuel cells," *Journal of The Electrochemical Society,* vol. 158, no. 4, pp. B416-B423, 2011.

[20] U. Beuscher, "Experimental method to determine the mass transport resistance of a polymer electrolyte fuel cell," *Journal of The Electrochemical Society,* vol. 153, no. 9, pp. A1788-A1793, 2006.

[21] D. A. Caulk and D. R. Baker, "Heat and water transport in hydrophobic diffusion media of PEM fuel cells," *Journal of The Electrochemical Society,* vol. 157, no. 8, pp. B1237-B1244, 2010.

[22] J. P. Owejan, T. A. Trabold *et al.*, "Oxygen transport resistance correlated to liquid water saturation in the gas diffusion layer of PEM fuel cells," *International Journal of Heat and Mass Transfer,* vol. 71, pp. 585-592, 2014.

[23] T. V. Reshetenko and J. St-Pierre, "Separation method for oxygen mass transport coefficient in gas and Ionomer phases in PEMFC GDE," *Journal of The Electrochemical Society,* vol. 161, no. 10, pp. F1089-F1100, 2014.

[24] R. O'hayre, S.-W. Cha *et al.*, *Fuel cell fundamentals*. John Wiley & Sons, 2016.

[25] T. Springer, T. Zawodzinski *et al.*, "Characterization of polymer electrolyte fuel cells using AC impedance spectroscopy," *Journal of the Electrochemical Society,* vol. 143, no. 2, pp. 587-599, 1996.

[26] F. Jaouen, G. Lindbergh *et al.*, "Transient techniques for investigating mass-transport limitations in gas diffusion electrodes II. Experimental characterization of the PEFC cathode," *Journal of The Electrochemical Society,* vol. 150, no. 12, pp. A1711-A1717, 2003.

[27] A. Kulikovsky and M. Eikerling, "Analytical solutions for impedance of the cathode catalyst layer in PEM fuel cell: Layer parameters from impedance spectrum without fitting," *Journal of Electroanalytical Chemistry,* vol. 691, pp. 13-17, 2013.

[28] T. E. Springer, T. Zawodzinski *et al.*, "Polymer electrolyte fuel cell model," *Journal of the electrochemical society,* vol. 138, no. 8, pp. 2334-2342, 1991.

[29] J.-R. Kim, S. Y. Jung *et al.*, "Investigation of degradation mechanisms of a high-temperature polymer-electrolyte-membrane fuel cell stack by electrochemical impedance spectroscopy," *Journal of Power Sources,* vol. 220, pp. 54-64, 2012.

[30] J. Chen, T. Matsuura *et al.*, "Novel gas diffusion layer with water management function for PEMFC," *Journal of Power Sources,* vol. 131, no. 1-2, pp. 155-161, 2004.

[31] D. W. Green and R. H. Perry, *Perry's Chemical Engineers' Handbook/edición Don W. Green y Robert H. Perry* (no. C 660.28 P47 2008.). 1973.

[32] E. Gauthier, Q. Duan *et al.*, "Water flow in, through, and around the gas diffusion layer," *Fuel Cells,* vol. 12, no. 5, pp. 835-847, 2012.

[33] S.-M. Park and J.-S. Yoo, "Peer reviewed: electrochemical impedance spectroscopy for better electrochemical measurements," ed: ACS Publications, 2003.

[34] X. Yuan, H. Wang *et al.*, "AC impedance technique in PEM fuel cell diagnosis—A review," *International Journal of Hydrogen Energy,* vol. 32, no. 17, pp. 4365-4380, 2007.

[35] R. Makharia, M. F. Mathias *et al.*, "Measurement of catalyst layer electrolyte resistance in PEFCs using electrochemical impedance spectroscopy," *Journal of The Electrochemical Society,* vol. 152, no. 5, pp. A970-A977, 2005.

[36] E. N. Fuller, P. D. Schettler *et al.*, "New method for prediction of binary gas-phase diffusion coefficients," *Industrial & Engineering Chemistry,* vol. 58, no. 5, pp. 18-27, 1966.

[37] R. B. Bird, "Transport phenomena," *Applied Mechanics Reviews,* vol. 55, no. 1, pp. R1-R4, 2002.

[38] H. Giesche, "Mercury porosimetry: a general (practical) overview," *Particle & particle systems characterization,* vol. 23, no. 1, pp. 9-19, 2006.

[39] A. Khursheed, "Scanning electron microscope," ed: Google Patents, 2007.

국 문 초 록

본 논문에서는 고분자전해질 연료전지의 핵심부품인 미세기공층(MPL)의 물성특성을 변화하여 성능을 개선하였다. 이를 통해 연료전지 양극에서 발생하는 산소환원반응을 개선하고, 부산물인 물의 배출을 원활하게 하며 전극으로써의 전기전도성을 향상시켜 성능개선에 대한 현상규명을 하고자 한다.

연료전지의 지속적인 성능 개선으로 인해 물 배출이 중요해짐에 따라 가스확산층의 설계를 물 관리에 초점을 맞추었다. 기존 연구를 통해 가스확산층 미세 기공층의 특성이 물관리 및 산소의 확산에 지대한 영향을 미친다는 것을 밝혀낸 바가 있다. 따라서 본 연구에서는 세가지 종류의 탄소입자를 사용하여 물리적 특성이 서로 다른 샘플을 제작하였다.

먼저, 입자의 크기가 상이한 두 가지 탄소입자 A3 와 A6 를 적용하여 미세기공층 內 기공지름의 크기가 다른 샘플을 제작하였다. 실험 편광곡선을 통해 기공지름의 상승으로 농도손실이 개선되는 것을 파악하였다. 원인 규명을 위해 한계전류밀도 측정을 통한 산소확산저항을 측정하였다. 본 실험 조건에서의 산소의 확산은 기공지름의 차이에 의해 변하지 않는다는 것을 증명하였다. 반면에 기공 지름의 상승은 모세관 압을 낮추어 물 배출이 용이해 지는 점이 농도손실의 개선점으로 파악되었다.

물의 배출이 중요해지는 고 가습조건에서 개선된 성능을 가진 탄소입자 A6 에 전기전도도가 향상된 탄소입자 C 를 점진적으로 함유시켜 연료전지의 성능을 개선하고자 하였다. 탄소입자 C 는 전기적 전도성이 뛰어난 대신, 비표면적이 A6 입자에 비해 10 배이상 크다는 특징을 가지고 있다. 임피던스 분광법을 통해 C 타입 탄소함량이 증가할수록 이온전도도를 포함한 옴 저항이 점진적으로 개선되는 결과를 보였다. 하지만 탄소화합물의 총 비표면적이 증가하며 농도손실의 착수가

빨라지는 결과를 보였다. C 타입 탄소의 함유량이 늘어날 수록 전류-전압 곡선과 임피던스 분광법을 통한 분석결과에서의 농도손실의 시작구간이 앞당겨지는 것을 확인하였으며 이 결과를 통해 전기전도성을 향상시키면서 농도손실을 최소화하는 최적 출력밀도를 도출하고자 하였다.

SEM 이미지 분석과 기공측정, 그리고 접촉각 측정 등 Ex-situ 시험 분석을 통해 물성의 특성을 파악하고 수치를 정량적으로 파악하였다. 이를 실험 모델에 반영하여 정량적인 분석을 진행하였다. 해당 실험 샘플 중 A6 타입 탄소분자에 3wt.%의 C 타입 탄소를 함유한 MPL 이 상용 샘플에 비교하여 1.16 배 상승한 출력밀도를 가진 것으로 확인하였다.

본 연구에서는 이론을 기반으로 한 미세기공층의 물성특성의 변화에 대한 성능의 변화 추이를 정량적으로 분석하였다. 기공지름과 전도성 탄소함유로 인한 성능변화의 원인규명을 한계전류밀도 측정과 임피던스 분광법을 통해 분석하여 이론을 바탕으로 설명하였다. 이는 추후 가스확산층및 이에 호환하는 핵심부품의 개발에 기여할 수 있을 것으로 보인다.

주요어: 미세기공층 (MPL), 고분자 전해질 연료전지 (PEMFC) 물 관리, 한계전류밀도, 임피던스 분광법, 산소전달저항,

학 번: 2016-23285